Downloaded from orbit.dtu.dk on: May 22, 2022

DTU Library

Unsteady 2D potential-flow forces on a thin variable geometry airfoil undergoing arbitrary motion

Gaunaa, M.

Publication date:
2006

Document Version
Publisher's PDF, also known as Version of record

Link back to DTU Orbit

Citation (APA):
Gaunaa, M. (2006). *Unsteady 2D potential-flow forces on a thin variable geometry airfoil undergoing arbitrary motion*. Denmark. Forskningscenter Risoe. Risoe-R No. 1478(EN)

General rights
Copyright and moral rights for the publications made accessible in the public portal are retained by the authors and/or other copyright owners and it is a condition of accessing publications that users recognise and abide by the legal requirements associated with these rights.

- Users may download and print one copy of any publication from the public portal for the purpose of private study or research.
- You may not further distribute the material or use it for any profit-making activity or commercial gain
- You may freely distribute the URL identifying the publication in the public portal

If you believe that this document breaches copyright please contact us providing details, and we will remove access to the work immediately and investigate your claim.

Risø-R Report

RISØ

Risø–R–1478(EN)

Unsteady 2D Potential-flow Forces on a Thin Variable Geometry Airfoil Undergoing Arbitrary Motion

Mac Gaunaa

Risø National Laboratory
Roskilde
Denmark
July 2006

Author: Mac Gaunaa
Title: Unsteady 2D Potential-flow Forces on a Thin Variable Geometry Airfoil Undergoing Arbitrary Motion
Department: Wind Energy Department

Risø–R–1478(EN)
July 2006

Abstract (max. 2000 char.):
In this report analytical expressions for the unsteady 2D force distribution on a variable geometry airfoil undergoing arbitrary motion are derived under the assumption of incompressible, irrotational, inviscid flow. The airfoil is represented by its camberline as in classic thin-airfoil theory, and the deflection of the airfoil is given by superposition of chordwise deflection mode shapes. It is shown from the expressions for the forces, that the influence from the shed vorticity in the wake is described by the same time-lag for all chordwise positions on the airfoil. This time-lag term can be approximated using an indicial function approach, making the practical calculation of the aerodynamic response numerically very efficient by use of Duhamel superposition. Furthermore, the indicial function expressions for the time-lag terms are formulated in their equivalent state-space form, allowing for use of the present theory in problems employing the eigenvalue approach, such as stability analysis.
The analytical expressions for the forces simplify to all previously known steady and unsteady thin-airfoil solutions. Apart from the obvious applications within active load control/reduction, the current theory can be used for various applications which up to now have been possible only using much more computational costly methods. The propulsive performance of a soft heaving propulsor, and the influence of airfoil camberline elasticity on the flutter limit are two computational examples given in the report that highlight this feature.

ISSN 0106-2840
ISBN 87–550–3369–5

Contract no.:

Group's own reg. no.:
(Føniks PSP-element)

Sponsorship:
Partly funded by the Danish Research Council under the ADAPWING project

Cover :

Pages: 52
Tables:
References: 23

Risø National Laboratory
Information Service Department
P.O.Box 49
DK-4000 Roskilde
Denmark
Telephone +45 46774004
bibl@risoe.dk
Fax +45 46774013
www.risoe.dk

Risø–R–1478(EN)

Unsteady 2D Potential-flow Forces on a Thin Variable Geometry Airfoil Undergoing Arbitrary Motion

Mac Gaunaa

Risø National Laboratory, Roskilde, Denmark
July 2006

Abstract In the present work analytical expressions for distributed and integral unsteady 2D forces on a variable geometry airfoil undergoing arbitrary motion are derived under the assumption of incompressible, irrotational, inviscid flow. The airfoil is represented by its camberline as in classic thin-airfoil theory, and the deflection of the airfoil is given by superposition of chordwise deflection mode shapes. It is shown from the expressions for the forces, that the influence from the shed vorticity in the wake is described by the same time-lag for all chordwise positions on the airfoil. This time-lag term can be approximated using an indicial function approach, making the practical calculation of the aerodynamic response numerically very efficient by use of Duhamel superposition. Furthermore, the indicial function expressions for the time-lag terms are formulated in their equivalent state-space form, allowing for use of the present theory in problems employing the eigenvalue approach, such as stability analysis.

The analytical expressions for the forces simplify to all previously known steady and unsteady thin-airfoil solutions.

Apart from the obvious applications within active load control/reduction, the current theory can be used for various applications which up to now have been possible only using much more computational costly methods. The propulsive performance of a soft heaving propulsor, and the influence of airfoil camberline elasticity on the flutter limit are two computational examples given in the report that highlight this feature.

ISBN 87–550–3369–5
ISSN 0106–2840

Print: Pitney Bowes Management Services Denmark A/S · 2006

Contents

Nomenclature *5*

1 Introduction *8*

2 Theoretical Model *9*
2.1 The Basics and Assumptions *9*
2.2 Non-Circulatory Normal Force and Moment *11*
2.3 Circulatory Normal Force and Moment *13*
2.4 Total Normal Force and Moment *16*
2.5 Local Pressure Difference Over the Airfoil *17*
2.6 Leading Edge Suction Force *18*
2.7 Tangential Force *19*
2.8 Power Required to Move the Airfoil *20*
2.9 Formulation Including Heaving and Pitching Motion *21*

3 Determination of Unsteady Wake Effects *22*
3.1 Equivalent State-Space Formulation *23*

4 Discussion *23*
4.1 Comparison with Previous Work *23*
4.2 Computational Example: Propulsive Performance of a Soft Heaving Propulsor *29*
4.3 Computational Example: Influence of Airfoil Camberline Elasticity on Flutter Limits *31*

5 Conclusions *38*

References *39*

Appendix *41*

A General Surface Velocity Potential *41*

B Full Force Expressions *42*

C Computation of the Deflection Shape Integrals *48*

D Velocity Potentials and Analytical Values of the Integrals Used for Computing Deflection Integrals for a Flat Plate With a Flap *51*

Nomenclature

Roman Letters

$\underline{\underline{\mathbf{A}}}$	coefficint matrix of first-order matrix equation, Eq. (141)	$-$
A_i	unit response constant, Eq. (77)	$-$
b	airfoil half-chord length	m
b_i	unit response time decay constant, Eq. (77)	$-$
b_0	amplitude of motion of thin swimming plate	m
$B1_0,\ B1_1$	Bessel functions of the first kind	$-$
$B2_0,\ B2_1$	Bessel functions of the second kind	$-$
c	non-dimensional chordwise coordinate	$-$
$\mathbf{C}$	Theodorsen's function	$-$
D	drag force	N
$\underline{\underline{\mathbf{D}}}$	damping matrix	$-$
$\underline{\mathbf{d}}$	aeroelastic states	$-$
$Defl_i(t)$	temporal modal amplitude for mode i	$-$
EI	bending stiffness	Nm^2
$f_{y,i}(c)$	deflection shape integral	m
$f_{dyd\varepsilon,i}(c)$	deflection shape integral	$-$
$F_{y,i}$	deflection shape integral	m
$F_{dyd\varepsilon,i}$	deflection shape integral	$-$
$G_{y,i}$	deflection shape integral	m
$G_{dyd\varepsilon,i}$	deflection shape integral	$-$
$H_{y,i}$	deflection shape integral	m
$H_{dyd\varepsilon,i}$	deflection shape integral	$-$
$\underline{\underline{\mathbf{I}}}$	identity matrix	$-$
I_a	moment of inertial around $\varepsilon = ab$	$kg\,m^2$
$I_{modal,i}$	integral, Equation 110	N/m
$I_{MSy,i}$	integral, Equation 109	kg
Ims_i	integral, Equation 127	kg
Ins_i	integral, Equation 120	kg
$\underline{\underline{\mathbf{K}}}$	stiffness matrix	$-$
$K_1(c),\ K_2(c)$	helping functions, Eq. (49)/(B.9) and (B.10)	$-$
$K_{y,i}$	deflection shape integral	m
$K_{dyd\varepsilon,i}$	deflection shape integral	$-$
k	reduced frequency	$-$
k_x	constant determining wavelength of swimming motion	$-$
L	lift force	N
l	cantilever beam length/vert. gust wave length	m
LES	leading edge suction force	N
M	moment	Nm
$\underline{\underline{\mathbf{M}}}$	mass matrix	$-$
M_D	damping moment	Nm
M_E	elastic moment	Nm
M_I	inertial moment	Nm
M_{tot}	total mass	kg
m	distributed mass	kg/m
m_i	modal mass	kg
$M_p(c)$	partial moment at non-dim coord c, from c to the trailing-edge	Nm
N	normal force	N
N_D	damping normal force	N
N_E	elastic normal force	N

N_I	inertial normal force	N
$N_p(c)$	partial normal force, from non-dim coord c to the trailing-edge	N
$Nterms$	number of terms	$-$
p	unsteady aerodynamic pressure	pa
$\tilde{p}$	sum of distr. aerodyn. force and local inertial force	pa
ΔP	pressure difference betw. lower and upper sides of airfoil	pa
P_{fict}	local fictitious inertial force from acc. of coord. syst.	pa
$PI1 - PI9$	req. power deflection shape integrals	
Pow	power required to perform airfoil motion	Nm/s
Q	Equivalent flat plate three-quarter downwash, Eq. (38)	m/s
s	non-dimensional time	$-$
T	tangential force	N
$\overline{T}$	mean thrust of swimming plate	N
t	time	s
$TI1 - TI9$	tang. force deflection shape integrals	
V	free-stream velocity	m/s
V_y	velocity normal to the airfoil chord, vertical gust velocity	m/s
W	half-amplitude of vertical gust	m/s
w	local flow velocity	m/s
X	displ. of the airfoil (ε, y) coord-syst. in free-stream dir.	m
$x,\ x_0,\ x_1,\ x_2$	non-dimensional chordwise coordinate $[-1..1]$	$-$
$\tilde{x}$	cantilever length parameter (clamped end 0, free end 1)	$-$
y	coordinate of airfoil camberline, dir. perp. to freestream	m
$\tilde{y}$	local y-coordinate of a pitching, heaving and deflecting airfoil	m
y_i	coordinate of deflection mode shapes, dir. perp. to freestream	m
Y	displ. of (ε, y) coord-syst. in dir. perp. to free-stream dir. (heave)	m
z_i	aerodynamic state variable	

Greek Letters

α	pitching motion displacement (angle of attack)	rad
γ	distributed vortex strength (local vortex sheet strength)	
δ	Kronecker delta	$-$
ε	dimensional chordwise coordinate, pos. towards trailing edge	m
η	propulsive eficiency	$-$
κ	non-dimensional mass	$-$
ν	frequency of vertical gust	rad
ξ_s	structural damping ratio	$-$
ρ	fluid density	kg/m^3
σ	distributed source strength	
φ	velocity potential	
ω	vibrational mode eigenfrequency	rad
Γ	concentrated point vortex strength	
Φ	circulatory force step response function	$-$

Indices

c	circulatory
$Defl$	deflection
$\dot{Defl}$	deflection velocity
$dyd\varepsilon$	variables obatained using y'
$hinge$	hinge point
LE	leading edge

$lower$	lower side of airfoil
nc	non-circulatory
p	partial
$upper$	upper side of airfoil
y	variables obatained using y
Y	heaving
$\dot{Y}$	heaving velocity
α	pitching
$\dot{\alpha}$	pitching velocity

Differentation Notation

$\dot{()} = \frac{\partial}{\partial t}()$	partial differentation with respect to time
$()' = \frac{\partial}{\partial \varepsilon}()$	partial differentation w. resp. to dimensional chordwise coord.

1 Introduction

Previous analytical and numerical investigations of unsteady aerodynamic forces on deformable airfoils are for the majority based on the two-dimensional potential-flow aerodynamic model of Theodorsen [20], which includes the aerodynamic effect of a flat trailing edge flap on a flat airfoil. Such efforts are found in the works of Leishman [17] and Hariharan et al. [11]. Other works dealing with deformations of the airfoil which are not flat trailing edge flaps have used more computational costly models, such as the discrete vortex method of Katz et al. [14, 15] or even full Navier-Stokes methods as in van der Wall et al. [21].

Another branch of investigations on the aerodynamic response for deformable thin surfaces concern swimming of fish. Within this field analytical results for the force response of harmonically waving 2D thin plates have been solved by Wu [22, 23]. In these works, focus is on the mechanics of swimming of fish, i.e. the propulsive efficiency of the harmonic motion, which include integrals over surface shape, pressure and leading edge force singularity in time and space.

One application of deformable airfoils is within the field of wind energy. It has been shown that active load reduction for MW size wind turbines can alleviate load increments from non-homogenous inflow considerably [2, 3, 4, 16]. With the development of smart materials such as piezoelectric materials, it is becoming possible to have active flow control by deformation of airfoil shapes. Up to now aerodynamic calculation of such problems have only been possible with computationally rather expensive methods, rendering aeroelastic and aeroservoelastic computations very time consuming in these cases. Recent two- and three-dimensional investigations using the present aerodynamic model [1, 5] have shown that there is a big potential of fatigue load reduction on wind turbines using airfoils with variable trailing edge geometry. The strength of variable geometry lies in the ability to obtain fast actuation speeds compared to the slower actuation speeds of conventional pitching systems on wind turbines. A continuous deformation of the airfoil trailing edge is aerodynamically more well behaved than a stiff trailing edge flap due to the absence of discontinuities in the surface curvature. Moreover, the aerodynamic noise generation using a continuously deformed airfoil is far lower than that of the rigid flap case due to the discontinuity of the surface curvature in the rigid flap case.

One branch of 2D potential-flow models for airfoils is the thin-airfoil theory, in which the airfoil is represented by its camberline. Despite the crude assumptions made in this theory, the results compare well with what is observed on thin airfoils when the flow is fully attached. Historic thin-airfoil works include Munk's [18] solution of the general stationary thin-airfoil problem in 1922, where he derived the normal force and moment on a thin airfoil of arbitrary shape. Milestones in unsteady thin-airfoil theory include the works by Glauert [9] and Theodorsen [20], where the lift and moment on flat thin airfoils with trailing edge flaps undergoing heaving and pitching motion were derived. The unsteady leading edge suction force was treated by Garrick [7], which made it possible to investigate the propulsive efficiency of oscillatory heaving, pitching and TE-flapping motions of a flat airfoil with a flat flap. Wu [22, 23] solved analytically the propulsive efficiency of harmonically waving thin plates in order to study the basic principle of fish propulsion.

In the present work, analytical expressions for the unsteady 2D force distribution on a variable geometry airfoil undergoing arbitrary motion is derived under the thin-airfoil potential-flow assumption. The time-lag term associated with the unsteady wake can be approximated using an indicial function approach, making the practical calculation of the aerodynamic response numerically very efficient by use of Duhamel superposition. The indicial function expressions can be restated in state-space form, as described by Hansen et al. [10]. The indicial and state-space expressions of the present model will both be

given in this report. It will be shown that the present model reduce to the expressions of Munk [18] and Theodorsen [20] in the case of steady flow over an airfoil of arbitrary shape and unsteady flow over a flat plate with a flat trailing edge flap, respectively. Comparisons of the propulsive efficiency predicted with the present algorithm is in excellent agreement with the analytical results of Garrick [7] and Wu [22] for a heaving flat plate and a progressing wave of given wavelength and phase velocity over the chord, respectively.

2 Theoretical Model

The airfoil is represented by its camberline as in classic thin-airfoil theory, and the deflection of the airfoil is given by superposition of chordwise deflection mode shapes. Furthermore, the airfoil can move in the direction of the oncoming flow. The derivation of the analytic expressions for the distribution of unsteady aerodynamic forces in the direction normal to the airfoil surface follows the lines of Theodorsen's [20] classic work from 1935. The singularity on the leading edge of the infinitely thin airfoil gives rise to a leading edge suction force, which can be considered the limit of the physical suction force for airfoil thickness going to zero. Using an analytic expression for the leading edge suction force, the airfoil tangential force and drag force are derived, integrating the contributions of aerodynamic forces on the curved airfoil. The approach used for deriving the tangential and drag forces is a generalization of the method used by Garrick [7]. The expression for the force distribution show that the dynamic response of the system is characterized by certain integrals involving the mode shapes and mode shape slopes, which can be calculated prior to time simulations.

It will be shown from the final expressions for the forces, that the influence from the shed vorticity in the wake can be described by the same time-lag for all chordwise positions on the airfoil. This time-lag term can be approximated using an indicial function approach, as first outlined by Von Karman et al. [13], making the practical calculation of the aerodynamic response numerically very efficient by use of Duhamel superposition. The indicial function expressions can be restated in state-space form, as described by Hansen et. al. [10]. The state-space expressions for the present model are also given in this report.

2.1 The Basics and Assumptions

The present model uses the usual 2D potential-flow assumptions, which are an incompressible, irrotational, inviscid fluid and 2D flow. This corresponds to very high Reynolds numbers, low mach-numbers and small angles of attack in real life. In this work the usual thin-airfoil approach is adopted. This means that the airfoil is represented by it's camberline only, and the thickness of the airfoil is therefore neglected. The free-stream flow velocity, V, is constant, but the airfoil may move in the direction of the free-stream.

The dimensional coordinates of the airfoil camberline are described in the (ε, y) coordinate system. The ε-axis is parallel with the the free-stream velocity, V, and can be translated in the ε-direction. The translation is given by X, but as it shall turn out later, only the first and the second order time derivatives of this quantity are needed in the model. Since the model is restricted to small deformations, the projected length of the airfoil on the ε-axis can be considered constant. The coordinate system is situated such that the airfoil mid-chord is at $\varepsilon = 0$. Therefore the airfoil leading edge is at $\varepsilon = -b$ and the airfoil trailing edge is at $\varepsilon = b$, where b is the airfoil half-chord length. In the derivations that follows, there will be frequent use of non-dimensional chordwise coordinates, x, defined by $x = \varepsilon/b$. Figure 1 shows the coordinate systems used in the present work.

The unsteady forces in a 2D potential-flow problem are determined from the pressures,

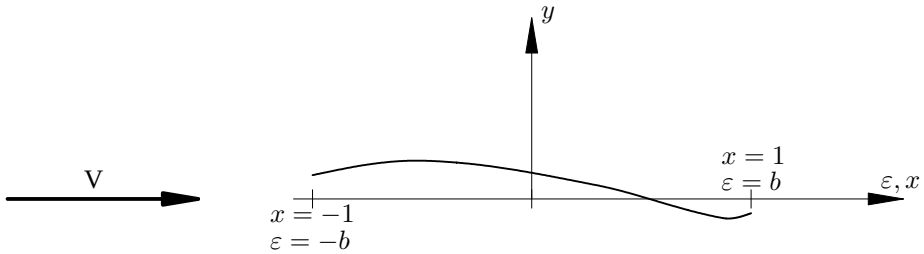

Figure 1: *Definition of dimensional and non-dimensional coordinate systems used in the present work.*

given by the unsteady Bernoulli equation,

$$p = -\rho\left(\frac{w^2}{2} + \dot{\varphi}(x,t)\right) + C. \tag{1}$$

Here w is the local flow velocity, ρ is the fluid density, and C is a constant. The dot, $\dot{()}$, signifies differentation with respect to time, $\frac{\partial}{\partial t}$, and φ is the velocity potential at the point where the pressure is evaluated.

In the special case of an infinitely thin airfoil, the surface velocity potential of the upper surface of the airfoil, φ, is a function of both time and chordwise position. The surface velocity potential of the lower surface is equal in magnitude to the upper one, but with opposite sign. The reason for this is apparent from the general derivation of the surface velocity potential in Appendix A, which will be used later in the derivation of the forces on the airfoil. The local flow velocity is given by

$$w = V - \dot{X}(t) + \varphi'(x,t), \tag{2}$$

where the prime, $()'$, signifies differentation with respect to the dimensional chordwise coordinate, $\frac{\partial}{\partial \varepsilon}$. $\dot{X}(t)$ is the velocity of the airfoil coordinate system in the direction of the free-stream, and V is the free-stream velocity. Substituting the local flow velocity, Equation (2), into the unsteady Bernoulli Equation (1), results in the pressure difference over the airfoil is obtained in Equation (3)

$$\Delta P(x) = p_{lower} - p_{upper} = 2\,\rho\left(\dot{\varphi}(x,t) + (V - \dot{X}(t))\varphi'(x,t)\right). \tag{3}$$

In the derivation of the above relation, it was used that the surface velocity potential on the upper and lower sides of the airfoil has opposite signs. The ordinary thin-airfoil assumption and result, that $\mid V \mid \gg \mid \varphi' \mid$ and that the surface velocity potential on the upper and lower sides of the airfoil has opposite signs, was used to arrive at Equation (3). The pressure difference between the airfoil lower and upper sides results in a force which is locally normal to the camberline. In the derivation of the normal force on the airfoil to follow, it is assumed that the local angle of the camberline with respect to the chordline is small, such that $y' \ll 1$.

An additional force is present at the leading edge of the airfoil. The solution of the normal force problem will show that there exist a singularity at the leading edge, corresponding to an infinitely low pressure. The force from this leading edge singularity corresponds to the limit of a pressure going toward infinity for a leading edge radius, and hence projected area, tending to zero. In the following derivation assumptions are that the influence from the airfoil on itself, and the influence from the unsteady wake on the airfoil can be determined as if the airfoil and the wake lie on a straight line.

In Theodorsen's [20] elegant derivation of the normal forces and moments acting on a plane airfoil with a flat flap, the total forces are spilt into forces from position/motion of the airfoil and forces from the velocity induced by the unsteady wake. These force terms were termed circulatory and non-circulatory, respectively. This splitting of the problem is used in the present work also.

Since the deflection of the airfoil is given by superposition of chordwise deflection mode shapes, the motion perpendicular to the free-stream direction at any point on the deformable airfoil can be described by a sum of these mode shapes

$$y(x,t) = \sum_{i=1}^{Ndefl} y_i(x) Defl_i(t) \tag{4}$$

The mode shapes $y_i(x)$ are a function of the chordwise coordinate only, whereas the scaling of these are determined by $Defl_i(t)$, which is a function of time only. The velocity and acceleration of any point of the surface in the y-direction is obtained by differentation of Equation (4) with respect to time

$$\dot{y}(x,t) = \sum_{i=1}^{Ndefl} y_i(x) \dot{Defl}_i(t) \tag{5}$$

$$\ddot{y}(x,t) = \sum_{i=1}^{Ndefl} y_i(x) \ddot{Defl}_i(t) \tag{6}$$

The number of deformation shapes are given by $Ndefl$. Note that solid body translation in the y-direction (heaving motion) and solid body rotation can be described in terms of deflection shapes; by one mode shape each. In order to keep the present formulation of the theory as short as possible, only the general form of the problem in terms of the deflection shapes are given in the main report. Expressions explicitly involving heaving motion, Y, and pitching (or rotational) motion, α, are given in Appendix B. Please note in the derivations to follow, that both x and x_1 coordinates are dimensionless, such that -1 and 1 correspond to the leading and trailing edges, respectively.

2.2 Non-Circulatory Normal Force and Moment

It is shown in Appendix A that a distributed sheet of sources with strength $\sigma(x_1,t)$ on the upper side of the airfoil, and a distributed sheet of sources of the opposite strength $(-\sigma(x_1,t))$ on the lower side of the infinitely thin airfoil corresponds to a surface velocity potential

$$\varphi(x,t) = \frac{b}{4\pi}\int_{-1}^{1} \sigma(x_1,t) \ln\left(\frac{(x-x_1)^2 + \left(\sqrt{1-x^2}-\sqrt{1-x_1{}^2}\right)^2}{(x-x_1)^2 + \left(\sqrt{1-x^2}+\sqrt{1-x_1{}^2}\right)^2}\right) dx_1 \tag{7}$$

on the upper surface of the airfoil. The velocity normal to the airfoil induced by the sheets of sources on the airfoil at chordwise coordinate x, is a function of the source/sink strength at x only:

$$V_y(x,t) = -\frac{\sigma(x,t)}{2}\,. \tag{8}$$

The velocity component normal to the airfoil due to the free-stream and motion of the airfoil in the X-direction is

$$V_y(x,t) = -\left(V - \dot{X}(t)\right) \sum_{i=1}^{Ndefl} Defl_i(t) y_i'(x) \tag{9}$$

The velocity component normal to the airfoil due to the deflection of the airfoil itself is

$$V_y(x,t) = \sum_{i=1}^{Ndefl} y_i(x) \dot{Defl}_i(t) \tag{10}$$

This means that the source/sink strength needed to enforce the Neumann boundary condition at the airfoil corresponds to the surface velocity potential

$$\varphi(x,t) = \varphi_{Defl}(x,t) + \varphi_{\dot{Defl}}(x,t) \tag{11}$$

$$\varphi_{Defl}(x,t) = \frac{b}{2\pi}\left(V-\dot{X}(t)\right)\sum_{i=1}^{Ndefl} Defl_i(t) f_{dyd\varepsilon,i}(x) \tag{12}$$

$$\varphi_{D\dot{e}fl}(x,t) = \frac{b}{2\pi}\sum_{i=1}^{Ndefl} D\dot{e}fl_i(t) f_{y,i}(x) \tag{13}$$

where $f_{y,i}(x)$ and $f_{dyd\varepsilon,i}(x)$ are given by

$$f_{y,i}(x) = \int_{-1}^{1} y_i(x_1)\ln\left(\frac{(x-x_1)^2+\left(\sqrt{1-x^2}-\sqrt{1-x_1{}^2}\right)^2}{(x-x_1)^2+\left(\sqrt{1-x^2}+\sqrt{1-x_1{}^2}\right)^2}\right)dx_1 \tag{14}$$

$$f_{dyd\varepsilon,i}(x) = \int_{-1}^{1} y_i'(x_1)\ln\left(\frac{(x-x_1)^2+\left(\sqrt{1-x^2}-\sqrt{1-x_1{}^2}\right)^2}{(x-x_1)^2+\left(\sqrt{1-x^2}+\sqrt{1-x_1{}^2}\right)^2}\right)dx_1 \tag{15}$$

Note that $f_{y,i}(x)$ and $f_{dyd\varepsilon,i}(x)$ are integrals that only depend on the deflection shape and the chordwise coordinate x. Therefore, they can be computed prior to a time simulation. These types of integrals are in the following denoted deflection shape integrals.

The forces perpendicular to the surface of the airfoil due to the motion of the airfoil are determined by inserting the velocity potential, Equation (11), into the unsteady Bernoulli equation applied to a thin airfoil, Equation (3). From this the integral partial non-circulatory normal forces and moments can be integrated.

$$N_{p,nc}(c) = b\int_{c}^{1} \Delta P(x)\,dx \tag{16}$$

$$M_{p,nc}(c) = -b^2\int_{c}^{1} (x-c)\,\Delta P(x)\,dx \tag{17}$$

Note that the partial normal force correspond to the contributions from the non-dimensional coordinate c to the trailing edge. Analogous, the partial moment $M_p(c)$ is the moment with respect to non-dimensional position c from the distributed normal forces from c to the trailing edge. Note also that the moment is positive nose-up. The force coefficients for the entire airfoil section is obtained by inserting $c=-1$ in the above equations:

$$N = N_p(-1) \tag{18}$$

$$M_{LE} = M_p(-1) \tag{19}$$

The moment above is taken with respect to the leading edge, but can be used to compute the moment at any desired point given by the non-dimensional coordinate c because

$$M(c) = M_{LE} + Nb(1+c) \tag{20}$$

The general expressions for the non-circulatory forces are obtained by filling in the expressions for the potentials into the above relations, which after considerable but trivial reduction yields

$$\begin{aligned}
N_{p,nc}(c) &= -2\,\rho\,b\left(V-\dot{X}(t)\right)\varphi(c,t) + 2\,\rho\,b\int_{c}^{1}\dot{\varphi}(x,t)dx \\
&= \frac{\rho\,b^2}{\pi}\Bigg(\sum_{i=1}^{Ndefl} D\ddot{e}fl_i(t)F_{y,i}(c) - \ddot{X}(t)\sum_{i=1}^{Ndefl} Defl_i(t)F_{dyd\varepsilon,i}(c) \\
&\qquad + \left(V-\dot{X}(t)\right)\sum_{i=1}^{Ndefl} D\dot{e}fl_i(t)F_{dyd\varepsilon,i}(c)\Bigg) \\
&\quad -\frac{\rho\,b}{\pi}\left(V-\dot{X}(t)\right)\Bigg(\left(V-\dot{X}(t)\right)\sum_{i=1}^{Ndefl} Defl_i(t)f_{dyd\varepsilon,i}(c)
\end{aligned}$$

$$+ \sum_{i=1}^{Ndefl} \dot{Defl}_i(t) f_{y,i}(c) \Bigg) \tag{21}$$

$$\begin{aligned}
M_{p,nc}(c) &= -2\,\rho\,b^2 \int_c^1 \dot{\varphi}(x,t)\,(x-c)\,dx + 2\,\rho\,b\,\left(V - \dot{X}(t)\right) \int_c^1 \varphi(x,t)dx \\
&= \frac{\rho\,b^3}{\pi} \ddot{X}(t) \sum_{i=1}^{Ndefl} Defl_i(t)\,(G_{dyd\varepsilon,i}(c) - cF_{dyd\varepsilon,i}(c)) \\
&\quad -\frac{\rho\,b^3}{\pi}\left(V - \dot{X}(t)\right) \sum_{i=1}^{Ndefl} \dot{Defl}_i(t)\,(G_{dyd\varepsilon,i}(c) - cF_{dyd\varepsilon,i}(c)) \\
&\quad +\frac{\rho\,b^2}{\pi}\left(V - \dot{X}(t)\right)^2 \sum_{i=1}^{Ndefl} Defl_i(t) F_{dyd\varepsilon,i}(c) \\
&\quad -\frac{\rho\,b^3}{\pi} \sum_{i=1}^{Ndefl} \dot{Defl}_i(t)\,(G_{y,i}(c) - cF_{y,i}(c)) \\
&\quad +\frac{\rho\,b^2}{\pi}\left(V - \dot{X}(t)\right) \sum_{i=1}^{Ndefl} \dot{Defl}_i(t) F_{y,i}(c)
\end{aligned} \tag{22}$$

where the deflection shape integrals $F_{y,i}(c)$, $G_{y,i}(c)$, $F_{dyd\varepsilon,i}(c)$ and $G_{dyd\varepsilon,i}(c)$ are given by

$$F_{y,i}(c) = \int_c^1 f_{y,i}(x)dx \tag{23}$$

$$G_{y,i}(c) = \int_c^1 x f_{y,i}(x)dx \tag{24}$$

$$F_{dyd\varepsilon,i}(c) = \int_c^1 f_{dyd\varepsilon,i}(x)dx \tag{25}$$

$$G_{dyd\varepsilon,i}(c) = \int_c^1 x f_{dyd\varepsilon,i}(x)dx \tag{26}$$

2.3 Circulatory Normal Force and Moment

The contribution of forces on a thin airfoil due to the unsteady wake was treated in Theodorsen's [20] classic work. The present treatment of the circulatory normal force and moment can be considered a generalization of Theodorsen's work.

There is at least two key elements in any potential-flow airfoil solution. The first element is the Neumann boundary condition, which state that there should be no flow through the airfoil surface. This element has already been used previously in the derivation of the non-circulatory forces, and is used in the derivation of the circulatory forces as well. The other key element in any potential-flow airfoil theory for attached flow is the Kutta condition, which requires that the trailing edge should not be a singularity. This can be considered an enforcement of a virtual viscosity at the trailing edge. In this case, the Kutta condition is equivalent to enforcing

$$\lim_{x \to b} |\partial\varphi(x,t)/\partial x| < \infty \tag{27}$$

For unsteady potential-flow solutions, there is one more key element, the Kelvin theorem, which states that the sum of the circulation in the two-dimensional universe should be zero. This means that any change in the circulation bound on the airfoil, the so called bound circulation, is reflected in the airfoil wake, where the opposite amount of circulation is shed from the trailing edge. As the airfoil in this case can move in the free-stream direction, the relative velocity of the vortex sheet with respect to the airfoil is $V - \dot{X}(t)$.

Since the derivation below follows closely Theodorsen's [20] classic derivation, the details are only briefly summarized here, and the interested reader is encouraged to consult Theodorsen's original work. As shown by Theodorsen, the velocity potential at non-dimensional x-coordinate x due to a concentrated vortex of strength $-\Delta\Gamma$ located at the ε-coordinate bx_0 is

$$\varphi_{x_0}(x) = -\frac{\Delta\Gamma}{2\pi}\arctan\left(\frac{\sqrt{1-x^2}\sqrt{1-x_0^2}}{1-xx_0}\right) \tag{28}$$

Since the relative velocity of the wake vorticity with respect to the airfoil is $V - \dot{X}(t)$, the time derivative of the velocity potential can be expressed

$$\frac{\partial\varphi}{\partial t} = \frac{\partial\varphi}{\partial x_0}(V - \dot{X}(t)) \tag{29}$$

Upon insertion into Equation (3), the corresponding pressure difference over the airfoil becomes

$$\Delta P(x) = 2\,\rho(V - \dot{X}(t))\left(\frac{\partial\varphi_\Gamma}{\partial x} + \frac{\partial\varphi_\Gamma}{\partial x_0}\right). \tag{30}$$

Theodorsen [20] further showed, that

$$\frac{\partial\varphi_\Gamma}{\partial x} = \frac{\Delta\Gamma}{2\pi}\sqrt{\frac{x_0^2-1}{1-x^2}}\left(\frac{1}{x_0-x}\right) \tag{31}$$

and

$$\frac{\partial\varphi_\Gamma}{\partial x_0} = \frac{\Delta\Gamma}{2\pi}\sqrt{\frac{x_0^2-1}{1-x^2}}\left(\frac{1}{x_0-x}\right) \tag{32}$$

Combining Equations (31) and (32), the following relation is obtained

$$\frac{\partial\varphi_\Gamma}{\partial x} + \frac{\partial\varphi_\Gamma}{\partial x_0} = \frac{\Delta\Gamma}{2\pi}\frac{x+x_0}{\sqrt{1-x^2}\sqrt{1-x_0^2}} \tag{33}$$

By inserting Equation (33) into Equation (30) and integrating from non-dimensional coordinate $x = c$ to the trailing edge $x = 1$, the partial circulatory normal force due to the concentrated wake vortex is obtained after some reduction

$$\begin{aligned}\Delta N_{p,c}(c) = \rho(V - \dot{X}(t))b\frac{\Delta\Gamma}{2\pi}\Bigg[&\frac{x_0}{\sqrt{x_0^2-1}}\left(\arccos(c) - \sqrt{1-c^2}\right)\\ &+\frac{\sqrt{x_0+1}}{\sqrt{x_0-1}}\sqrt{1-c^2}\Bigg]\end{aligned} \tag{34}$$

If $\gamma(x_0)$ is the strength of the distributed vorticity in the wake at non-dimensional position x_0, then the partial normal force due to the whole wake is obtained from integration of Equation (34) by setting $\Delta\Gamma = b\gamma(x_0)dx_0$,

$$\begin{aligned}N_{p,c}(c) &= \int_1^\infty \Delta N_{p,c}(c)dx_0\\ &= \frac{\rho(V - \dot{X}(t))b}{\pi}\Bigg[\left(\arccos(c) - \sqrt{1-c^2}\right)\int_1^\infty \frac{x_0}{\sqrt{x_0^2-1}}\gamma(x_0)dx_0\\ &\qquad + \sqrt{1-c^2}\int_1^\infty \frac{\sqrt{x_0+1}}{\sqrt{x_0-1}}\gamma(x_0)dx_0\Bigg]\end{aligned} \tag{35}$$

The derivation of the partial circulatory moment is analog to the derivation of the partial circulatory normal force. The partial moment is

$$M_{p,c} = -\frac{\rho(V - \dot{X}(t))b^2}{\pi}\times$$

$$\left[\left(\sqrt{1-c^2}(1+c/2)-\arccos(c)(c+1/2)\right)\int_1^\infty \frac{x_0}{\sqrt{x_0^2-1}}\gamma(x_0)dx_0\right.$$

$$\left.+1/2\left(\arccos(c)-c\sqrt{1-c^2}\right)\int_1^\infty \frac{\sqrt{x_0+1}}{\sqrt{x_0-1}}\gamma(x_0)dx_0\right] \tag{36}$$

In order to arrive at something more directly useful, the Kutta condition is employed. For this use, the circulatory velocity potential shall be needed. This is obtained from integration of Equation (31)

$$\frac{\partial\varphi_\Gamma}{\partial x} = \frac{1}{2\pi}\int_1^\infty \sqrt{\frac{x_0^2-1}{1-x^2}}\left(\frac{1}{x_0-x}\right)(V-\dot{x})\,dx_0 \tag{37}$$

Inserting the non-circulatory velocity potential, Equation (11), and the circulatory velocity potential, Equation (37), into the Kutta condition, Equation (27), the important relation is obtained

$$Q=\frac{1}{2\pi}\int_1^\infty \frac{\sqrt{x_0+1}}{\sqrt{x_0-1}}\gamma(x_0)dx_0 = -\frac{1}{2\pi}\left(V-\dot{X}(t)\right)\sum_{i=1}^{Ndefl} Defl_i(t)H_{dyd\varepsilon,i}$$

$$-\frac{1}{2\pi}\sum_{i=1}^{Ndefl}\dot{Defl}_i(t)H_{y,i} \tag{38}$$

Q can be interpreted as an equivalent flat plate three-quarter downwash, because if mode shapes corresponding to heave and pitching motion of a flat airfoil is inserted into Equation (38), Q is recognized as the downwash in the three-quarter-chord point on the airfoil; a quantity which is essential for computation of the unsteady aerodynamic response for rigid airfoils. The deflection shape integrals $H_{y,i}$ and $H_{dyd\varepsilon,i}$ are given by

$$H_{y,i} = -2\int_{-1}^{1}\frac{y_i(x_1)\sqrt{1-x_1{}^2}}{x_1-1}dx_1 \tag{39}$$

$$H_{dyd\varepsilon,i} = -2\int_{-1}^{1}\frac{y_i'(\varepsilon)\sqrt{1-x_1{}^2}}{x_1-1}dx_1 \tag{40}$$

Using Equation (38), which links the wake vorticity distribution to the airfoil deformation states, the partial circulatory normal force and moment, Equations (35) and (36) can be rewritten into a more convenient form

$$N_{p,c}(c) = 2\,b\rho\left(V-\dot{X}(t)\right)\left(\arccos(c)-\sqrt{1-c^2}\right)Q\mathbf{C}$$

$$+2\,b\rho\left(V-\dot{X}(t)\right)\left(-\frac{1}{2\pi}\left(V-\dot{X}(t)\right)\sum_{i=1}^{Ndefl} Defl_i(t)H_{dyd\varepsilon,i}\right.$$

$$\left.-\frac{1}{2\pi}\sum_{i=1}^{Ndefl}\dot{Defl}_i(t)H_{y,i}\right)\sqrt{1-c^2} \tag{41}$$

$$M_{p,c}(c) = -2\,b^2\rho\left(V-\dot{X}(t)\right)\left(\sqrt{1-c^2}\,(1+1/2\,c)\right.$$

$$\left.-\arccos(c)\,(c+1/2)\right)Q\mathbf{C}$$

$$-2\,b^2\rho\left(V-\dot{X}(t)\right)\left(1/2\,\arccos(c)-1/2\,c\sqrt{1-c^2}\right)Q \tag{42}$$

In the equations above, **C** is Theodorsen's [20] function,

$$\mathbf{C} = \frac{\int_1^\infty \frac{x}{\sqrt{x^2-1}}\gamma(x)dx}{\int_1^\infty \frac{x+1}{\sqrt{x^2-1}}\gamma(x)dx} \tag{43}$$

which can be considered a renormalization function to take into account the effect of the unsteady wake. As previously, the total circulatory normal force and moment can be obtained by setting $c=-1$ in the expressions.

2.4 Total Normal Force and Moment

The total partial normal force is obtained by adding the non-circulatory and circulatory parts, Equations (21) and (41). The result is

$$
\begin{aligned}
N_p(c) \quad = \quad & \frac{\rho\, b^2}{\pi}\Bigg(\sum_{i=1}^{Ndefl} D\ddot{e}fl_i(t) F_{y,i}(c) - \ddot{X}(t) \sum_{i=1}^{Ndefl} Defl_i(t) F_{dyd\varepsilon,i}(c) \\
& \qquad + \left(V - \dot{X}(t)\right) \sum_{i=1}^{Ndefl} D\dot{e}fl_i(t) F_{dyd\varepsilon,i}(c) \Bigg) \\
& + 2\, b\rho \left(V - \dot{X}(t)\right) \left(\arccos(c) - \sqrt{1-c^2}\right) Q\mathbf{C} \\
& - b\rho \sqrt{1-c^2} \left(V - \dot{X}(t)\right) \Bigg(\frac{\left(V - \dot{X}(t)\right) \sum_{i=1}^{Ndefl} Defl_i(t) H_{dyd\varepsilon,i}}{\pi} \\
& \qquad + \frac{\sum_{i=1}^{Ndefl} D\dot{e}fl_i(t) H_{y,i}}{\pi} \Bigg) \\
& - \rho\, b \left(V - \dot{X}(t)\right) \Bigg(\frac{\left(V - \dot{X}(t)\right) \sum_{i=1}^{Ndefl} Defl_i(t) f_{dyd\varepsilon,i}(c)}{\pi} \\
& \qquad + \frac{\sum_{i=1}^{Ndefl} D\dot{e}fl_i(t) f_{y,i}(c)}{\pi} \Bigg)
\end{aligned}
\tag{44}
$$

The full integral normal force is obtained by setting $c = -1$ in the equation above

$$
\begin{aligned}
N \quad = \quad & \frac{\rho b^2}{\pi} \sum_{i=1}^{Ndefl} \Big(D\ddot{e}fl_i(t) F_{y,i}(-1) - \ddot{X} Defl_i(t) F_{dyd\varepsilon,i}(-1) \\
& \qquad + (V - \dot{X}) D\dot{e}fl_i(t) F_{dyd\varepsilon,i}(-1) \Big) \\
& + 2\pi\rho b (V - \dot{X}) \cdot Q\mathbf{C}
\end{aligned}
\tag{45}
$$

The total partial moment with respect to c is obtained by adding Equations (22) and (42).

$$
\begin{aligned}
M_p(c) \quad = \quad & \rho b^3 \frac{1}{\pi} \ddot{X}(t) \sum_{i=1}^{Ndefl} Defl_i(t) \left(G_{dyd\varepsilon,i}(c) - c F_{dyd\varepsilon,i}(c) \right) \\
& + \rho b^2 \frac{1}{\pi} (V - \dot{X}(t))^2 \sum_{i=1}^{Ndefl} Defl_i(t) F_{dyd\varepsilon,i}(c) \\
& + \rho b^2 (V - \dot{X}(t))^2 \frac{K_1(c)}{2\pi} \sum_{i=1}^{Ndefl} Defl_i H_{dyd\varepsilon,i} \\
& - \rho b^3 \frac{1}{\pi} (V - \dot{X}(t)) \sum_{i=1}^{Ndefl} D\dot{e}fl_i(t) (G_{dyd\varepsilon,i}(c) - c F_{dyd\varepsilon,i}(c)) \\
& + \rho b^2 \frac{1}{\pi} (V - \dot{X}(t)) \sum_{i=1}^{Ndefl} D\dot{e}fl_i(t) F_{y,i}(c) \\
& + \rho b^2 (V - \dot{X}(t)) \frac{K_1(c)}{2\pi} \sum_{i=1}^{Ndefl} D\dot{e}fl_i(t) H_{y,i} \\
& - \rho b^3 \frac{1}{\pi} \sum_{i=1}^{Ndefl} D\ddot{e}fl_i(t) (G_{y,i}(c) - c F_{y,i}(c))
\end{aligned}
\tag{46}
$$

$$+2\rho b^2(V-\dot{X}(t))\left((c+1/2)\arccos(c)-(1+c/2)\sqrt{1-c^2}\right)Q\mathbf{C}$$

The moment from the whole airfoil acting around the point defined by the non-dimensional chordwise coordinate $x=a$ is

$$M = M_c(-1)-(a+1)bN \tag{47}$$

This results for the integral moment around the point defined by the non-dimensional chordwise coordinate $x=a$

$$\begin{aligned}
M = {} & \rho b^3\frac{1}{\pi}\ddot{X}(t)\sum_{i=1}^{Ndefl} Defl_i(t)\left(G_{dyd\varepsilon,i}(-1)-aF_{dyd\varepsilon,i}(-1)\right) \\
& +\rho b^2\frac{1}{\pi}(V-\dot{X}(t))^2\sum_{i=1}^{Ndefl} Defl_i(t)F_{dyd\varepsilon,i}(-1) \\
& +\rho b^2(V-\dot{X}(t))^2\frac{1}{2}\sum_{i=1}^{Ndefl} Defl_iH_{dyd\varepsilon,i} \\
& -\rho b^3\frac{1}{\pi}(V-\dot{X}(t))\sum_{i=1}^{Ndefl} D\dot{e}fl_i(t)(G_{dyd\varepsilon,i}(-1)-aF_{dyd\varepsilon,i}(-1)) \\
& +\rho b^2\frac{1}{\pi}(V-\dot{X}(t))\sum_{i=1}^{Ndefl} D\dot{e}fl_i(t)F_{y,i}(-1) \\
& +\rho b^2(V-\dot{X}(t))\frac{1}{2}\sum_{i=1}^{Ndefl} D\dot{e}fl_i(t)H_{y,i} \\
& -\rho b^3\frac{1}{\pi}\sum_{i=1}^{Ndefl} D\ddot{e}fl_i(t)(G_{y,i}(-1)-aF_{y,i}(-1)) \\
& +2\pi\rho b^2(V-\dot{X}(t))(1/2+a)Q\mathbf{C}
\end{aligned} \tag{48}$$

Where the function $K_1(c)$ is given by

$$K_1(c) = \pi/2-c\sqrt{1-c^2}-\arcsin c=\arccos(c)-c\sqrt{1-c^2} \tag{49}$$

All the integrals involved in the expressions are constant in time, and can be computed prior to time simulations, thus making the computations numerically efficient.

2.5 Local Pressure Difference Over the Airfoil

The local pressure difference over the airfoil can be obtained from differentation of the partial normal force with respect to the evaluation point c.

$$\begin{aligned}
N_c(c) &= b\int_c^1 \Delta P(x_1)dx_1 \\
&\Updownarrow \\
\frac{\partial N_c(c)}{\partial c} &= -b\Delta P(c) \\
&\Updownarrow \\
\Delta P(c) &= -1/b\frac{\partial N_c(c)}{dc}
\end{aligned} \tag{50}$$

This results in the following local pressure difference over the airfoil

$$\Delta P(c) = \rho b\frac{1}{\pi}\left(\sum_{i=1}^{Ndefl} D\ddot{e}fl_i(t)f_{y,i}(c)\right.$$

$$
\begin{aligned}
&-\ddot{X}(t)\sum_{i=1}^{Ndefl} Defl_i(t) f_{dyd\varepsilon,i}(c) \\
&+(V-\dot{X}(t))\sum_{i=1}^{Ndefl} D\dot{e}fl_i(t) f_{dyd\varepsilon,i}(c)\Bigg) \\
&-2\rho(V-\dot{X}(t))\frac{c-1}{\sqrt{1-c^2}}Q\mathbf{C} \qquad (51)\\
&-\rho\frac{1}{\pi}(V-\dot{X}(t))^2\Bigg(\frac{c}{\sqrt{1-c^2}}\sum_{i=1}^{Ndefl} Defl_i(t) H_{dyd\varepsilon,i} \\
&\qquad -\sum_{i=1}^{Ndefl} Defl_i(t)\frac{\partial f_{dyd\varepsilon,i}(c)}{\partial c}\Bigg) \\
&-\rho\frac{1}{\pi}(V-\dot{X}(t))\Bigg(\frac{c}{\sqrt{1-c^2}}\sum_{i=1}^{Ndefl} D\dot{e}fl_i(t) H_{y,i} \\
&\qquad -\sum_{i=1}^{Ndefl} D\dot{e}fl_i(t)\frac{\partial f_{y,i}(c)}{\partial c}\Bigg)
\end{aligned}
$$

Note that the time-lag effect from the wake is described by the same quantity, $Q\mathbf{C}$, on all points on the airfoil. This enables very efficient computations of unsteady pressure differences for the deformable airfoil.

2.6 Leading Edge Suction Force

It is seen from the expression for the pressure difference over the airfoil, Equation (51), that there exist a singularity at the leading edge of the airfoil. This singularity on the infinitely thin airfoil gives rise to an infinitely low pressure at the leading edge. Athough clearly not physical, this can be considered the limit of the physical suction force for airfoil thickness going to zero. Garrick [7] treated this problem for the flat airfoil with a flat flap. The present treatment of the leading edge suction force can be considered a generalization of his work. In Durand [6], the limit value of the suction force for the thickness approaching zero is given as

$$
LES = \pi\rho S^2 \qquad (52)
$$

$$
S = \lim_{x\to -1^+}\left(\frac{\sqrt{b}}{2}\sqrt{x+1}\,\gamma(x)\right) \qquad (53)
$$

In Equation (53) above, $\gamma(x)$ is the vorticity distribution on the thin airfoil, which in terms of the surface velocity potential used in this work corresponds to $2\varphi'(x)$. As previously, the prime, $()'$, signifies differentation with respect to the dimensional chordwise coordinate. The value of S is finite, since it can be shown that $\varphi'(x)$ is infinite in the order of $1/\sqrt{1+x}$ at the leading edge, $x=-1$. Using the relation

$$
\gamma(x) = 2\varphi'(x) = \frac{2}{b}\frac{\partial\varphi(x)}{\partial x}
$$

in combination with the expressions for the potential, Equations (11) and (37), the equivalent flat plate three-quarter downwash, Equation (38), and the definition of Theodorsen's renormalization function, Equation (43), one obtains after reduction

$$
S = \sqrt{\frac{b}{2}}\Bigg(2\,Q\mathbf{C} + \frac{V-\dot{X}(t)}{2\pi}\sum_{i=1}^{Ndefl} Defl_i(t)\left(K_{dyd\varepsilon,i}+H_{dyd\varepsilon,i}\right)
$$

$$+\frac{1}{2\pi}\sum_{i=1}^{Ndefl}\dot{Defl}_i(t)\left(K_{y,i}+H_{y,i}\right)\Bigg) \tag{54}$$

The deflection shape integrals $K_{y,i}$ and $K_{dyd\varepsilon,i}$ are given by

$$K_{y,i} = -2\int_{-1}^{1}\frac{y_i(x_1)\sqrt{1-x_1{}^2}}{x_1+1}dx_1 \tag{55}$$

$$K_{dyd\varepsilon,i} = -2\int_{-1}^{1}\frac{y_i'(x_1)\sqrt{1-x_1{}^2}}{x_1+1}dx_1 \tag{56}$$

The final expression for the leading edge suction force is obtained by inserting Equation (54) into Equation (52). The final result is for the leading edge suction force is

$$\begin{aligned} LES &= \frac{\pi}{2}\rho b\Bigg(2Q\mathbf{C}+\frac{V-\dot{X}(t)}{2\pi}\sum_{i=1}^{Ndefl}Defl_i(t)(K_{dyd\varepsilon,i}+H_{dyd\varepsilon,i}) \\ &\quad +\frac{1}{2\pi}\sum_{i=1}^{Ndefl}\dot{Defl}_i(t)(K_{y,i}+H_{y,i})\Bigg)^2 \end{aligned} \tag{57}$$

2.7 Tangential Force

The tangential force consists of a contribution from the leading edge suction force and a contribution from the pressure difference over the airfoil projected onto the tangential force direction.

$$T = LES + \sum_{i=1}^{Ndefl}Defl_i\int_{-1}^{1}b\,\Delta P(x_1)\frac{\partial y_i}{\partial\varepsilon}(x_1)dx_1 \tag{58}$$

The result is, after reduction

$$\begin{aligned} T &= \frac{\pi}{2}\rho b\Bigg(2Q\mathbf{C}+\frac{V-\dot{X}(t)}{2\pi}\sum_{i=1}^{Ndefl}Defl_i(t)(K_{dyd\varepsilon,i}+H_{dyd\varepsilon,i}) \\ &\qquad +\frac{1}{2\pi}\sum_{i=1}^{Ndefl}\dot{Defl}_i(t)(K_{y,i}+H_{y,i})\Bigg)^2 \\ &\quad +\rho b^2\frac{1}{\pi}\Bigg(\sum_{i=1}^{Ndefl}\sum_{j=1}^{Ndefl}Defl_i(t)\ddot{Defl}_j(t)TI2_{i,j} \\ &\qquad -\ddot{X}(t)\sum_{i=1}^{Ndefl}\sum_{j=1}^{Ndefl}Defl_i(t)Defl_j(t)TI3_{i,j} \\ &\qquad +(V-\dot{X}(t))\sum_{i=1}^{Ndefl}\sum_{j=1}^{Ndefl}Defl_i(t)\dot{Defl}_j(t)TI3_{i,j}\Bigg) \\ &- 2b\rho(V-\dot{X}(t))Q\mathbf{C}\sum_{i=1}^{Ndefl}Defl_i(t)TI5_i \\ &- 2\rho b(V-\dot{X}(t))\Bigg(\frac{(V-\dot{X}(t))}{2\pi}\sum_{i=1}^{Ndefl}\sum_{j=1}^{Ndefl}Defl_i(t)Defl_j(t)H_{dyd\varepsilon,j}TI7_i \\ &\qquad -\frac{(V-\dot{X}(t))}{2\pi}\sum_{i=1}^{Ndefl}\sum_{j=1}^{Ndefl}Defl_i(t)Defl_j(t)TI8_{i,j} \end{aligned}$$

$$+\frac{1}{2\pi}\sum_{i=1}^{Ndefl}\sum_{j=1}^{Ndefl} Defl_i(t)D\dot{e}fl_j(t)H_{y,j}TI7_i$$

$$-\frac{1}{2\pi}\sum_{i=1}^{Ndefl}\sum_{j=1}^{Ndefl} Defl_i(t)D\dot{e}fl_j(t)TI9_{i,j}\Bigg) \tag{59}$$

Where the deflection shape integrals corresponding to the tangential force are

$$TI2_{i,j} = \int_{-1}^{1} f_{y,j}(x_1)\, y_i'(x_1)dx_1 \tag{60}$$

$$TI3_{i,j} = \int_{-1}^{1} f_{dyd\varepsilon,j}(x_1)\, y_i'(x_1)dx_1 \tag{61}$$

$$TI5_i = \int_{-1}^{1} \frac{x_1-1}{\sqrt{1-x_1^2}}\, y_i'(x_1)dx_1 \tag{62}$$

$$TI7_i = \int_{-1}^{1} \frac{x_1}{\sqrt{1-x_1^2}}\, y_i'(x_1)dx_1 \tag{63}$$

$$TI8_{i,j} = \int_{-1}^{1} \frac{\partial f_{dyd\varepsilon,j}}{\partial x}(x_1)\, y_i'(x_1)dx_1 \tag{64}$$

$$TI9_{i,j} = \int_{-1}^{1} \frac{\partial f_{y,j}}{\partial x}(x_1)\, y_i'(x_1)dx_1 \tag{65}$$

Note that the numbering of the indexing on the TI-terms were developed with heave and pitching motion included explicitly in the formulation, which explains the peculiar numbering of the shown TI-terms in this shorter version of the formulation. The formulation of the forces with heave and pitch explicitly included in the equations are given in Appendix B. This is explained in Section 2.9.

2.8 Power Required to Move the Airfoil

The power required to perform any given motion of the airfoil can be computed. The external forces needed are equal and opposite to the pressure force across the plate. Therefore the power required to perform any motion is

$$Pow(t) = -\int_{-b}^{b} \Delta P(\varepsilon/b)\dot{y}(\varepsilon/b,t)d\varepsilon \tag{66}$$

Upon substituting non-dimensional coordinates and the mode shape formulation of the deflection velocity, Equation (5), the power required is

$$\begin{aligned} Pow(t) &= -b\int_{-1}^{1} \Delta P(x)\sum_{i=1}^{Ndefl} y_i(x)D\dot{e}fl_i(t)dx \\ &= -b\sum_{i=1}^{Ndefl} D\dot{e}fl_i(t)\int_{-1}^{1}\Delta P(x)y_i(x)dx \end{aligned} \tag{67}$$

After inserting the expression for the pressure difference over the plate, Equation (51), and rearranging, the final expression of the power required to move the airfoil reads

$$Pow = -\rho b^2\frac{1}{\pi}\Bigg(\sum_{i=1}^{Ndefl}\sum_{j=1}^{Ndefl} D\dot{e}fl_i(t)D\ddot{e}fl_j(t)PI2_{i,j}$$

$$-\ddot{X}(t)\sum_{i=1}^{Ndefl}\sum_{j=1}^{Ndefl} D\dot{e}fl_i(t)Defl_j(t)PI3_{i,j}$$

$$
\begin{aligned}
& +(V-\dot{X}(t)) \sum_{i=1}^{Ndefl} \sum_{j=1}^{Ndefl} \dot{Defl}_i(t)\dot{Defl}_j(t) PI3_{i,j} \Bigg) \\
+ \quad & 2b\rho(V-\dot{X}(t))Q\mathbf{C} \sum_{i=1}^{Ndefl} \dot{Defl}_i(t) PI5_i \\
+ \quad & 2\rho b(V-\dot{X}(t)) \Bigg(\frac{(V-\dot{X}(t))}{2\pi} \sum_{i=1}^{Ndefl} \sum_{j=1}^{Ndefl} \dot{Defl}_i(t) Defl_j(t) H_{dyd\varepsilon,j} PI7_i \\
& -\frac{(V-\dot{X}(t))}{2\pi} \sum_{i=1}^{Ndefl} \sum_{j=1}^{Ndefl} \dot{Defl}_i(t) Defl_j(t) PI8_{i,j} \\
& +\frac{1}{2\pi} \sum_{i=1}^{Ndefl} \sum_{j=1}^{Ndefl} \dot{Defl}_i(t) \dot{Defl}_j(t) H_{y,j} PI7_i \\
& -\frac{1}{2\pi} \sum_{i=1}^{Ndefl} \sum_{j=1}^{Ndefl} \dot{Defl}_i(t) \dot{Defl}_j(t) PI9_{i,j} \Bigg)
\end{aligned} \tag{68}
$$

The corresponding deflection shape integrals are analog to the tangential force deflection shape integrals with $y_i'(x_1)$ replaced by $y_i(x_1)$

$$PI2_{i,j} = \int_{-1}^{1} f_{y,j}(x_1)\, y_i(x_1) dx_1 \tag{69}$$

$$PI3_{i,j} = \int_{-1}^{1} f_{dyd\varepsilon,j}(x_1)\, y_i(x_1) dx_1 \tag{70}$$

$$PI5_i = \int_{-1}^{1} \frac{x_1 - 1}{\sqrt{1-x_1^2}}\, y_i(x_1) dx_1 \tag{71}$$

$$PI7_i = \int_{-1}^{1} \frac{x_1}{\sqrt{1-x_1^2}}\, y_i(x_1) dx_1 \tag{72}$$

$$PI8_{i,j} = \int_{-1}^{1} \frac{\partial f_{dyd\varepsilon,j}}{\partial x}(x_1)\, y_i(x_1) dx_1 \tag{73}$$

$$PI9_{i,j} = \int_{-1}^{1} \frac{\partial f_{y,j}}{\partial x}(x_1)\, y_i(x_1) dx_1 \tag{74}$$

2.9 Formulation Including Heaving and Pitching Motion

The formulation of the theory so far has been kept in a general formulation using the concept of deformation mode shapes. Most problems of interest within airfoil aerodynamics very often deal with heave and pitching motion, which very conveniently can be expressed in terms of deformation mode shapes. The deformation mode shape corresponding to a unit heaving motion is

$$y_Y(x) = 1$$

In this case the mode shape scaling coefficient is identical to the heaving coordinate $Defl_Y(t) = Y(t)$. If the pitching axis is given by the non-dimensional coordinate a, such that $a = -1$ and $a = 1$ corresponds to the leading and trailing edges, respectively, the (nose-up positive) unit deformation mode is

$$y_\alpha(x) = ba - x$$

For this case $Defl_\alpha(t) = \alpha(t)$. The velocity potentials corresponding to deflection and deflection velocity of these deformation mode shapes can be computed analytically from

Equations (12) and (13). The result is

$$\begin{aligned}
\varphi_Y(x) &= 0 \\
\varphi_{\dot{Y}}(x) &= -\dot{Y} b\sqrt{1-x^2} \\
\varphi_\alpha(x) &= (V-\dot{X})\alpha b\sqrt{1-x^2} \\
\varphi_{\dot{\alpha}}(x) &= \dot{\alpha} b^2(\frac{1}{2}x-a)\sqrt{1-x^2}
\end{aligned}$$

If these are inserted explicitly in all equations up to this chapter, the result is formulations explicitly including heaving and pitching motion. These are listed in Appendix B. In the derivations of these, the analytical values of some of the integrals given in Appendix D were used. The lift and drag values can be computed from the normal and tangential forces given in the appendix using the standard thin-airfoil assumptions $\alpha \ll 1$ and $D \ll L$.

$$L = N \tag{75}$$

$$D = -T + \alpha N \tag{76}$$

3 Determination of Unsteady Wake Effects

It was shown in the classic Von Karman and Sears paper [13], that it is possible to express terms of the type $Q\mathbf{C}$ in Equation (45) by superposition of step responses. In the case that the step response can be approximated by an exponential expression,

$$\Phi = 1 - \sum_{i=1}^{N_{terms}} A_i \exp(-b_i s) \tag{77}$$

$$s = 1/b \int_0^t (V - \dot{X}(t))dt, \tag{78}$$

this response can be computed numerically very efficiently. This is known as the indicial function concept, and results in the following equations for determination of $Q\mathbf{C}$

$$Q\mathbf{C} = Q(t)\left(1 - \sum_i A_i\right) + \sum_i z_i \tag{79}$$

where

$$z_i(t) = \frac{b_i A_i}{b}\int_0^t Q(t')(V-\dot{X}(t'))\exp\left(-\frac{b_i}{b}\int_{t'}^t V - \dot{X}(\tau)d\tau\right)dt'. \tag{80}$$

From the equation above, it can be seen that

$$\begin{aligned}
z_i(t+\Delta t) &= \exp(-b_i\Delta s)\cdot z_i(t) \\
&\quad + \frac{b_i A_i}{b}\int_t^{t+\Delta t} Q(t')(V-\dot{X}(t'))\exp\left(-\frac{b_i}{b}\int_{t'}^{t+\Delta t}\left(V-\dot{X}(\tau)\right)d\tau\right)dt'
\end{aligned} \tag{81}$$

where

$$\Delta s = \frac{1}{b}\int_t^{t+\Delta t}(V-\dot{X}(t'))dt'. \tag{82}$$

This means that each of the state variables z_i at any time is the value at the previous timestep multiplied by a decay factor plus an increment, a very cheap operation compared to a direct numerical integration of the integral it approximates. The accuracy of the method can be increased by using more than the commonly used two terms. For most tasks of engineering interest, however, a two-term approximation is sufficiently accyrate.

3.1 Equivalent State-Space Formulation

As shown by Hansen et.al. [10], it is possible to reformulate an indicial model such as the one described above in a state-space formulation. By differentation of Equation (80) with respect to time, it is seen that

$$\dot{z}_i + b_i \frac{1}{b}(V - \dot{X}(t))z_i \quad = \quad b_i A_i \frac{1}{b}(V - \dot{X}(t))Q(t). \tag{83}$$

This is the state-space model equivalent to the indicial function approximation of the unsteady aerodynamics, which is used in combination with Equation (79) to determine the time-lag effect due to the unsteady wake.

4 Discussion

The two main advantages of the model for the unsteady forces on a deforming airfoil presented in this work is its computational efficiency for time domain computations and the possibility to use the model directly in stability analysis because it can be formulated in a state-space representation. It is seen from the expressions for the forces on the airfoil that the time-lag effect associated with the wake vorticity can be expressed in terms of the term $Q\mathbf{C}$ on all forces, both local and integrated. The indicial function formulation of the unsteady wake effects combined with the evaluation of the deflection shape integrals prior to the time simulation loops makes time simulations with the present theory computationally very efficient. A rough comparison with the unsteady panel code of Gaunaa [8] showed that the present model is more than two orders of magnitude faster than the panel code for a time simulation with 1000 time steps. This ratio increases with the number of time steps, as the computational cost per timestep due to the summation over the wake vortices increases with the number of timesteps simulated. Since some of the deflection shape integrals require integration over singular expressions, calculation of these require special attention in order to limit numerical errors. One approach is to assume piecewise linear deflection shapes. This way the integrals can be computed from elementary solutions for linear deflection shapes. This method is elaborated in Appendix C.

The current theory is used in a more practical application by Buhl et al. [5] and Andersen [1], for assessment of the load reduction potential using airfoils with variable trailing edge geometry. Apart from the obvious applications within active load reduction, the current theory can be used for various applications, such as for instance investigation of airfoil softness on stability limits on the classical flutter case, which up to now have been possible only using much more computational costly methods.

In the following section, the present model is compared with previous work, after which two sections highlighting the versailty of the developed theory are found: Propulsive performance of a soft heaving propulsor, and influence of airfoil camberline elasticity on flutter limits.

4.1 Comparison with Previous Work

The present theory will be compared with earlier potential-flow thin-airfoil models which can be considered a simplification of the present model. Furthermore, results from an implementation of the model in Matlab will be compared to other models.

The expressions for normal force and moment will be compared with Munk's [18] expressions in the steady case. For the unsteady case with a flat airfoil with a flat flap, Theodorsen's [20] expressions are used as a reference. d'Alembert's paradox, zero drag for any steady two-dimensional potential-flow solution, is investigated, after which computational results for the propulsive efficiency of a heaving plate are compared with Garrick's [7] analytical results. Sears' [19] results are used to investigate how the present

model can handle a harmonic velocity gust in the direction perpendicular to the free-stream. As the last, and most complex test case, the results of Wu[22, 23] for the propulsive efficiency of a swimming plate will be used to compare how well the present model predicts the unsteady distributed forces, power, and leading edge suction force, since Wu's analytical work covered all these areas. Let's first proceed to the comparison with Munk's expressions for the normal force and moment for a steady thin airfoil of arbitrary shape.

Steady lift and moment, Munk's equations

The derived general expressions for normal forces and moments can be shown to reduce to Munk's [18] results in the steady case. The steady version of the normal force and moment, Equations (45) and (48) is

$$N = -\rho b V^2 \sum_{i=1}^{Ndefl} Defl_i(t) H_{dyd\varepsilon,i} \tag{84}$$

$$\begin{aligned} M &= \rho b^2 V^2 \frac{1}{\pi} \sum_{i=1}^{Ndefl} Defl_i(t) F_{dyd\varepsilon,i}(-1) \\ &\quad + \rho b^2 V^2 \frac{1}{2} \sum_{i=1}^{Ndefl} Defl_i H_{dyd\varepsilon,i} \\ &\quad + b(1/2 + a) N \end{aligned} \tag{85}$$

If now the shape of the airfoil is expressed as only one single deformation shape deformed to $Defl_1 = 1$, and the moment around the mid-chord, $a = 0$, is sought, then the equations further simplify to

$$N = -\rho b V^2 H_{dyd\varepsilon} \tag{86}$$

$$M = \rho b^2 V^2 \frac{1}{\pi} F_{dyd\varepsilon}(-1), \tag{87}$$

where $H_{dyd\varepsilon}$ and $F_{dyd\varepsilon}(-1)$ are

$$H_{dyd\varepsilon} = -2 \int_{-1}^{1} \frac{y'(x_1)\sqrt{1 - {x_1}^2}}{x_1 - 1} dx_1 \tag{88}$$

$$F_{dyd\varepsilon}(-1) = \int_{-1}^{1}\int_{-1}^{1} y'(x_2) \ln\left(\frac{(x_1 - x_2)^2 + \left(\sqrt{1 - {x_1}^2} - \sqrt{1 - {x_2}^2}\right)^2}{(x_1 - x_2)^2 + \left(\sqrt{1 - {x_1}^2} + \sqrt{1 - {x_2}^2}\right)^2}\right) dx_2\, dx_1 \tag{89}$$

By use of the relation $\sqrt{1 - x^2}/(x - 1) = -(x + 1)/\sin(\arccos(x))$ and the substitution $x = \cos(\tau)$ in combination with partial integration, the normal force can be rewritten to

$$N = 2\rho V^2 \int_{-1}^{1} \frac{y(z)}{(1 - z)\sqrt{1 - z^2}}\, dz, \tag{90}$$

which is exactly the formulation used by Munk. Likewise, it can be shown, that

$$F_{dyd\varepsilon}(-1) = -\frac{2\pi}{b} \int_{-1}^{1} \frac{\partial y}{\partial x_1} \sqrt{1 - x_1^2} dx_1 \tag{91}$$

As was the case for the normal force, this can be used with partial integration to recast the expression for the moment into

$$M = -2\rho V^2 b \int_{-1}^{1} \frac{y(z) z}{\sqrt{1 - z^2}}\, dz, \tag{92}$$

which was the exact formulation of Munk. Thus, the present theory reduces to Munk's expressions for normal force and moment for steady conditions.

Lift and moment on unsteady flat airfoil with a flat flap, Theodorsen's results

The classic investigation of the flutter phenomenon by Theodorsen [20] included determination of the unsteady aerodynamic lift, moment and flap moment for heaving, pitching and trailing edge flap motion. The velocity potentials corresponding to the heaving and pitching motions were described in Chapter 2.9. The velocity potential due to the motion of the trailing edge flap can be computed from Equations (12) and (13). This was done analytically by Theodorsen [20], and the results can be found in Appendix D. As the present theory builds on small deflections (including α), and therefore that $\mid N \mid \gg \mid T \mid$, the lift can be expressed as $L = N$. The normal force for the case including heave and pitch can be found from Equation (B.2) in Appendix B. Likewise, the moment and flap moment can be found from Equations (B.4) and (B.3). Upon insertion of the velocity potential due to the motion of the flat trailing edge flap, the forces can be found by help of the analytical integrals given in Appendix D. The result from this is identical to the results given by Theodorsen [20].

Zero steady drag, d'Alembert's paradox

It can be shown analytically by using the integrals given in Appendix D, that d'Alembert's paradox, zero drag for all steady potential flows, holds true for an uncambered airfoil with a flat trailing edge flap. However, the author has not yet been able to prove generally that the steady drag is zero using the present theory.

Propulsive efficiency of a heaving plate

Figure 2 shows a comparison between Garricks's [7] analytical results for the propulsive efficiency of the heaving plate, $\eta = V\overline{T}/\overline{Pow}$, and the results for the same problem computed with the present method[1]. It is seen that the agreement is very good. The slight difference between the present model and the analytical results is explained by the exponential step response function approximation, which in this case consist of only two terms. Higher accuracy is achievable with more terms. Two terms, however, are sufficient for most problems of engineering interest. The present results were computed using mean values over the last of 10 simulated oscillation periods with a temporal discretization of 100 time steps per oscillation period.

Sinusoidal vertical gust, Sears' function

The analytical solution to the sinusoidal vertical gust problem was solved by Sears [19]. It is possible to numerically solve the response for a vertical gust of arbitrary shape using a slightly modified version of the present model. The driving mechanism in all thin-airfoil potential-flow models is the flow normal to the airfoil camberline, so if N unit mode shapes corresponding to unit displacement velocities at N collocation points on the airfoil surface, respectively, and all terms corresponding to the slope of the airfoil is set to zero ($f_{dyd\varepsilon} = F_{dyd\varepsilon} = G_{dyd\varepsilon} = H_{dyd\varepsilon} = K_{dyd\varepsilon} = TI1-9 = 0$), the force output from the present theory corresponds to the forces due to an arbitrary forcing. The input to this model is the N vertical gust timeseries corresponding to the chordwise collocation point positions. Setting the vertical gust velocities to the real part of

$$V_y(x,t) \quad = \quad We^{i\nu(t-x/V)}$$

[1]Note that the overlines in the definition of η refer to mean values over the oscillation period after the initial transients have subsided

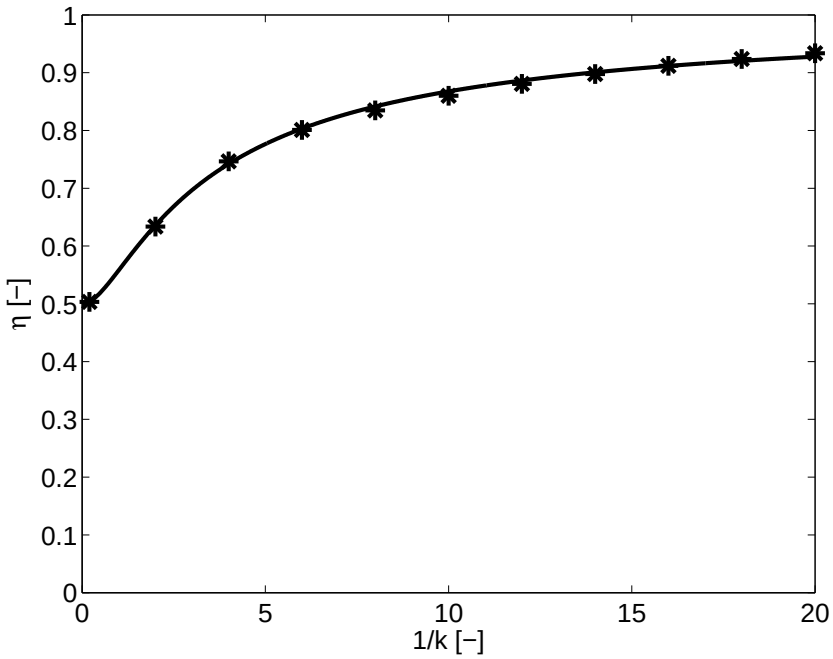

Figure 2: *Comparison of the analytical results of Garrick [7] (line) with results obtained using the present theory (stars) for a heaving flat plate. Propulsive efficiency,* η*, versus inverse wave number,* $1/k$*.*

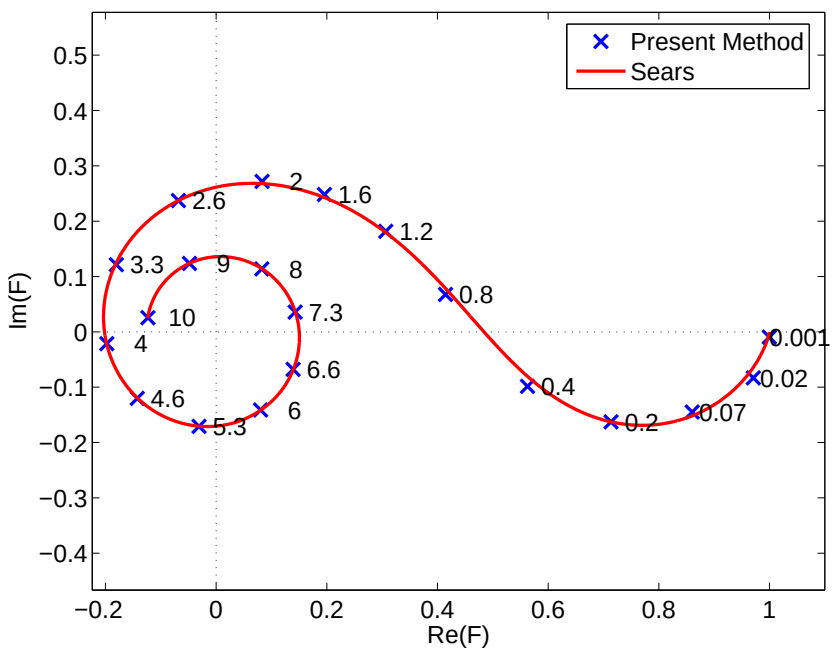

Figure 3: *Comparison of the analytical results of Sears [19] (curve) with results obtained using the present theory (x) for a flat plate . Imaginary versus real part of the function* $F(k)$ *(Equation (93)). The numbers on the figure signify the reduced frequency,* $k = \nu b/V$*, of the sinusoidal gust.*

corresponds to a sinusoidal vertical gust with amplitude $2W$ moving past the airfoil with the free-stream velocity, V. If the wave length of the gusts is l, the frequency, ν, with which the waves pass any point of the airfoil is

$$\nu = 2\pi V l$$

Sears' analytical solution to the problem is

$$\begin{aligned} L &= 2\pi\rho b V W e^{i\nu t} F(k) \\ F(k) &= \frac{B1_0(k)B2_1(ik) + i\,B1_1(k)B2_0(ik)}{B2_1(ik) + B2_0(ik)}, \end{aligned} \tag{93}$$

where $k = \nu b/V$ is the reduced frequency, i is the imaginaty unit, and $B1$ and $B2$ are Bessel functions of first and second kind, respectively. Using an equidistant chordwise resolution of $N = 100$ produces the result in Figure 3, where also the analytical solution of Sears [19] is shown. For each value of k, a vector drawn from the origin to the curve in the figure represents the lift in both magnitude and phase. A horizontal vector directed to the right is in phase with the gust velocity at the midpoint of the airfoil. It is seen that the results from the present method is in good agreement with those of Sears [19]. The explanation for the small difference between the present method and Sears' results is again attributed to the exponential response function approximantion. The present results are computed with the classic two-term approximation suggested by Jones [12].

Swimming of a thin plate

The analytical solution to the response to a deformation of the plate

$$y(x,t) = b_0 \cos(\omega t - k_x x), \qquad -1 < x < 1. \tag{94}$$

was derived by Wu [22]. The equivalent mode shape representation of this is

$$y(x,t) = \sum_{i=1}^{2} y_i(x) Defl_i(t), \tag{95}$$

where the mode shapes and deflection terms are

$$y_1(x) = \cos(k_x x) \tag{96}$$

$$y_2(x) = \sin(k_x x) \tag{97}$$

$$Defl_1(t) = b_0 \cos(\omega t) \tag{98}$$

$$Defl_2(t) = b_0 \cos(\omega t - \pi/2) \tag{99}$$

Wu's analytic solution showed that the mean values of thrust produced and power required to perform the motion is

$$\overline{T} = \pi\rho V^2 b_0^2 T_1(k, k_x) \tag{100}$$

$$\overline{Pow} = \pi\rho V^3 b_0^2 P_1(k, k_x) \tag{101}$$

for the swimming plate where the half-chord length is $b = 1$. The functions T_1 and P_1 were derived by Wu [22], and are functions of reduced frequency, k, and k_x. Figure 4 shows a comparison between Wu's analytical results for the waving plate and the results for the same problem computed with the present method. The non-dimensional frequency, k is

$$k = \frac{\omega b}{V}. \tag{102}$$

and the swimming efficiency is defined as in the case of the heaving plate

$$\eta = V\frac{\overline{T}}{\overline{Pow}}. \tag{103}$$

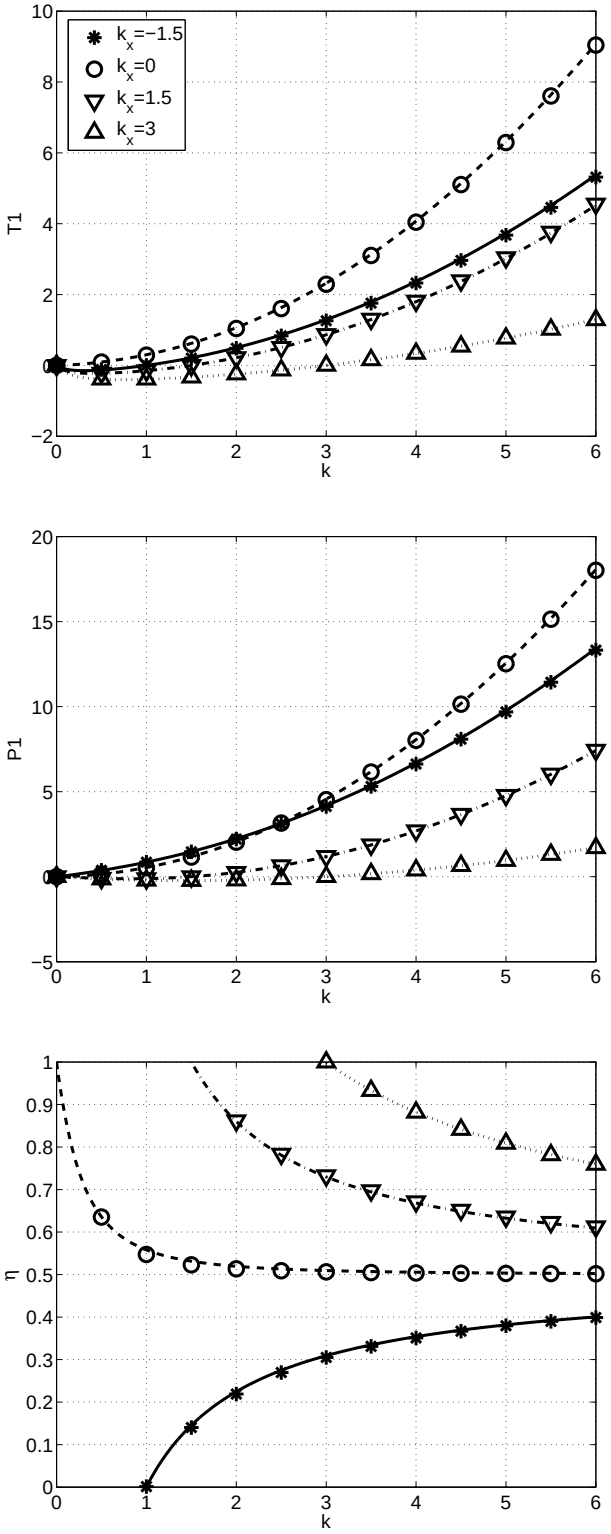

Figure 4: *Comparison of the analytical results of Wu [22] (lines) with results obtained using the present theory (symbols) for a waving plate with four different wavelengths of the swimming motion. Upper graph: Thrust versus reduced frequency, k. Middle graph: Power required to maintain the motion versus k. Lower graph: Swimming efficiency versus k*

It is seen from Figure 4 that the agreement with the analytical results for thrust, required power and swimming efficiency is excellent. The present results were obtained with a chordwise discretization of 101 points evenly spaced, 20 oscillation periods simulated, and 100 time steps per oscillation period. Note that when the velocity with which the deformation shape moves over the airfoil is equal to the relative flow velocity, corresponding to $k = k_x$, the forces on the airfoil are zero. This is due to the flow being undisturbed by the infinitely thin airfoil, corresponding to the zero angle of attack case in classic thin-airfoil theory.

4.2 Computational Example: Propulsive Performance of a Soft Heaving Propulsor

A computation of the aeroelastic response of an elastic thin heaving airfoil will be shown as an example of the possibilities presented by the present theory. Up to now fully aeroelastic analysis involving aeroelastic deformations of the lifting surface such as this has been possible only using much more computationally heavy methods such as for instance panel methods or full Navier-Stokes methods.

The heaving thin airfoil is actuated by an external force such that the angle of the leading edge is kept equal to zero, while the heave coordinate, Y, is varied harmonically in time. The equation for the deformation of an elastic two-dimensional plate is

$$\frac{\partial^2}{\partial \varepsilon^2}\left[EI(\varepsilon)\frac{\partial^2 y(\varepsilon/b,t)}{\partial \varepsilon^2}\right] + m(\varepsilon)\frac{\partial^2 y(\varepsilon/b,t)}{\partial t^2} + c\frac{\partial y(\varepsilon/b,t)}{\partial t} \quad = \quad \tilde{p}(\varepsilon), \tag{104}$$

where the distributed force $\tilde{p}(\varepsilon)$ is the sum of the distributed aerodynamic force, Equation (B.5), and the fictitious forces from the acceleration of the coordinate system in which the equation for the deformation of the elastic body is described.

$$\tilde{p}(\varepsilon) \quad = \quad \Delta P(\varepsilon/b) - \ddot{Y}(t)m(\varepsilon) \tag{105}$$

If the free vibration mode shapes corresponding to a cantilever beam is used to express the deformation of the plate, Equation (4), standard modal decomposition techniques can be used to express the elastic response of the system, Equation (104), as

$$m_i D\ddot{e}fl_i + 2m_i\omega_i\xi_s D\dot{e}fl_i + m_i\omega_i^2 Defl_i \quad = \quad \int_{-b}^{b} y_i(\varepsilon/b)\tilde{p}(\varepsilon)dx, \tag{106}$$

where the modal mass m_i is

$$m_i \quad = \quad \int_{-b}^{b} y_i(\varepsilon/b)^2 m(\varepsilon)dx \tag{107}$$

Note that $y_i(\varepsilon/b)$ and ω_i are the vibrational modes and their corresponding eigenfrequencies, and ξ_s is the structural damping ratio. Upon inserting $\dot{X} = \ddot{X} = \alpha = \dot{\alpha} = \ddot{\alpha} = 0$, Equation (105) and Equation (B.5) into the integral in Equation (106) and performing the integration, it is seen that

$$\begin{aligned} m_i D\ddot{e}fl_i \quad &+ \quad 2m_i\omega_i\xi_s D\dot{e}fl_i \;+\; m_i\omega_i^2 Defl_i \\ &= \quad b\sum_{i=1}^{Ndefl}\left(Defl_i I_{modal,i}\right) - b\, I_{MSy,i}\,\ddot{Y}, \end{aligned} \tag{108}$$

$I_{MSy,i}$ and $I_{modal,i}$ are expressed as

$$I_{MSy,i} \quad = \quad \int_{-1}^{1} y_i x_1 m x_1 dx_1 \tag{109}$$

$$I_{modal,i} \quad = \quad \int_{-1}^{1} \Delta P(x_1) y_i(x_1) dx_1$$

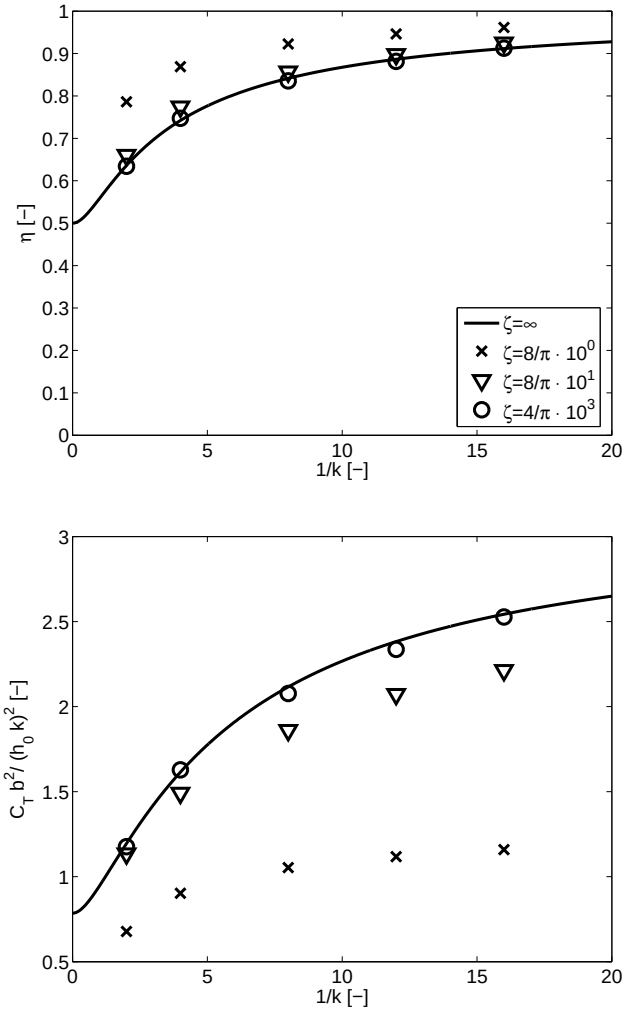

Figure 5: *Influence of reduced frequency on propulsive efficiency, η, (upper graph) and thrust (lower graph) for different stiffness coefficients, ζ, of the plate. The non-dimensional mass is $\kappa = M_{tot}/(\pi\rho b^2) = 0.1$. b_0 is the amplitude of the heaving motion. The results for $\eta = \infty$ is Garrick's [7] analytical solution.*

$$
\begin{aligned}
= \quad & -2\rho b\ddot{Y}PI1_i - 2\rho V\, Q\mathbf{C}\, PI5_i \\
& +\rho b\frac{1}{\pi}\left(\sum_{j=1}^{Ndefl} D\ddot{e}fl_j(t)PI2_{i,j} + V\sum_{j=1}^{Ndefl} D\dot{e}fl_j(t)PI3_{i,j}\right) \\
& -2\rho V\left(\frac{V}{2\pi}\sum_{j=1}^{Ndefl} Defl_j(t)(H_{dyd\varepsilon,j}PI7_i - PI8_{i,j})\right. \\
& \qquad \left. +\frac{1}{2\pi}\sum_{j=1}^{Ndefl} D\dot{e}fl_j(t)(H_{y,j}PI7_i - PI9_{i,j})\right) \qquad (110)
\end{aligned}
$$

Note that the Integrals in $I_{modal,i}$ are the same as in the expressions for computation of the power. The $Ndefl$ second order differential equations describing the modal deflections due to the heave forcing can be rewritten to $2 \cdot Ndefl$ first order differential equations, which can be solved in a straightforward way using standard ODE techniques. The shown results are obtained using the *ODE45* function in Matlab.

Figure 5 show the effect of the frequency, in terms of reduced frequency $k = \omega b/V$, and the stiffness, in terms of the non-dimensional parameter $\zeta = EI/(M_{tot}V^2b^2)$, on the propulsive efficiency, $\eta = V\overline{T}/\overline{Pow}$, and thrust produced. The non-dimensional mass in the example is $\kappa = M_{tot}/(\pi\rho b^2) = 0.1$. Only the first two deflection modes was used in the computations since the relative difference in propulsive efficiency from two to three deflection modes was below 0.5 percent for the softest case considered. The results were obtained by simulating 10 oscillation periods and using the mean values from the last period. It is seen that the results tend to the rigid plate results of Garrick [7] as the stiffness is increased. In agreement with the computations of Katz and Weihs [14] on large amplitude motion, a softer plate increases the propulsive efficiency and decreases the thrust for all frequencies.

Since the model for the forces, moments and modal forces is a linear system if the motion in the direction of the free-stream flow is neglected, the present theory makes possible stability investigations using the eigenvalue approach. Therefore, investigations of the effect of airfoil chordwise deformability on the flutter limits of a thin airfoil can be investigated if the airfoil is locked in the direction of the oncoming flow. This case is investigated in the next section.

4.3 Computational Example: Influence of Airfoil Camberline Elasticity on Flutter Limits

In this section the influence of airfoil softness on the flutter velocity is investigated. As in the previous section, the computations of this type have been possible only using computationally much heavier methods.

The classic flutter problem consists of a thin airfoil extending from $\varepsilon = -b$ to $\varepsilon = b$. The thin airfoil is hinged to a linear spring-damper system in heave and torsion at $\varepsilon = ab$, and has mass M_{tot} and moment of intertia I_a around $\varepsilon = ab$. This was solved by Theodorsen [20] in 1936, and is treated in detail in many textbooks on aeroelasticity.

Consider now the corresponding case where the thin airfoil is flexible. Approximating the small deformations of the airfoil by a modal expansion of the first $Ndefl$ orthogonal free vibration shapes of a flexible airfoil clamped at $\varepsilon = ab$ (corresponding to non-dimensional coordinate $x = a$)

$$y(x,t) = \sum_{i=1}^{Ndefl} y_i(x) Defl_i(t) \tag{111}$$

$$\dot{y}(x,t) = \sum_{i=1}^{Ndefl} y_i(x) \dot{Defl}_i(t) \tag{112}$$

$$\ddot{y}(x,t) = \sum_{i=1}^{Ndefl} y_i(x) \ddot{Defl}_i(t), \tag{113}$$

the motion of any point on the airfoil in the direction perpendicular to the free-stream velocity can be expressed in terms of the heave coordinate, Y, and the torsion coordinate α at the hinge point $\varepsilon_{hinge} = ab$.

$$\tilde{y}(\varepsilon,t) = Y(t) - \alpha(t)(\varepsilon - ab) + \sum_{i=1}^{Ndefl} y_i(\varepsilon/b) Defl_i(t) \tag{114}$$

$$\dot{\tilde{y}}(\varepsilon,t) = \dot{Y}(t) - \dot{\alpha}(t)(\varepsilon - ab) + \sum_{i=1}^{Ndefl} y_i(\varepsilon/b) \dot{Defl}_i(t) \tag{115}$$

$$\ddot{\tilde{y}}(\varepsilon,t) = \ddot{Y}(t) - \ddot{\alpha}(t)(\varepsilon - ab) + \sum_{i=1}^{Ndefl} y_i(\varepsilon/b)\ddot{Defl}_i(t) \tag{116}$$

Again, the torsion coordinate is assumed small. Alternatively, the heave and torsion coordinates could have been expressed in terms of their unit deflection terms, and the total motion of the system be cast into the general form of Equations (111) to (113). This would, however, make the following less transparent, so it is proceeded here using Equations (114) to (116).

Heaving motion equation

The equation for the heaving motion is derived from the normal force balance between inertial, elastic, damping and aerodynamic forces. The local inertial normal forces are given by

$$dN_I(\varepsilon) = -m(\varepsilon)\ddot{\tilde{y}}(\varepsilon,t) \tag{117}$$

Where $m(\varepsilon)$ is the local mass per unit depth. Integrating Equation (117) over the airfoil yields the integral inertial normal force

$$\begin{aligned} N_I &= \int_{-b}^{b} -m(\varepsilon)\ddot{\tilde{y}}(\varepsilon,t)d\varepsilon \\ &= -M_{tot}\ddot{Y}(t) - M_{tot}\ddot{\alpha}(t)(ab - \varepsilon_{cg}) - b\sum_{i=1}^{Ndefl} \ddot{Defl}_i(t)Ins_i \end{aligned} \tag{118}$$

where the integrals ε_{cg} (the ε-coordinate of the center of gravity) and Ins_i are given by

$$\varepsilon_{cg} = 1/M_{tot}\int_{-b}^{b} \varepsilon m(\varepsilon)d\varepsilon \tag{119}$$

$$Ins_i = 1/b\int_{-b}^{b} y_i(\varepsilon/b)m(\varepsilon)d\varepsilon = \int_{-1}^{1} y_i(x)m(xb)dx \tag{120}$$

The elastic and damping forces in the heaving direction are

$$N_E = -K_yY(t) \tag{121}$$

$$N_D = -C_y\dot{Y}(t), \tag{122}$$

and the external normal force, which in this case is the aerodynamic normal force, N, is given by Equation (45) with $\dot{X} = \ddot{X} = 0$. Alternatively, the heave (Y) and pitch (α) motions can be explicitly included in the formulation using Equation (B.2) in Appendix B in stead of Equation (45). The normal forces should be in equilibrium with each other

$$\begin{aligned} N_I + N_E + N_D + N &= 0 \\ &\Updownarrow \\ M_{tot}\ddot{Y} + C_y\dot{Y} + K_yY + M_{tot}(ab - \varepsilon_{cg})\ddot{\alpha} - N_{fict} - N &= 0 \end{aligned} \tag{123}$$

where the normal forces due to the deformation of the airfoil, N_{fict}, is

$$N_{fict} = -b\sum_{i=1}^{Ndefl}\left(\ddot{Defl}_i(t)Ins_i\right) \tag{124}$$

Pitching motion equation

Analogous to the equations for the heaving motion, the equations for the pitching motion is derived from the moment balance between inertial, elastic, damping and aerodynamic forces. In this case the moment is taken with respect to the elastic hinge point $x = ab$. The moment from the inertial forces are obtained from the distributed normal forces, Equation (117), as follows

$$\begin{aligned} M_I &= \int_{-b}^{b} dM_I \\ &= \int_{-b}^{b} (ab-\varepsilon) dN_I \\ &= -\int_{-b}^{b} (ab-\varepsilon) m(\varepsilon) \ddot{\dot{Y}}(\varepsilon/b, t) d\varepsilon \\ &= -M_{tot}(ab-\varepsilon_{cg})\ddot{Y} - I_a\ddot{\alpha} + abN_{fict} + b^2 \sum_{i=1}^{Ndefl} D\ddot{e}fl_i Ims_i \end{aligned} \tag{125}$$

Here I_a, the inertial moment around the hinge point $\varepsilon = ab$, and Ims_i are

$$I_a = \int_{-b}^{b} (\varepsilon - ab)^2 m(\varepsilon) d\varepsilon \tag{126}$$

$$Ims_i = 1/b^2 \int_{-b}^{b} y_i(\varepsilon/b) m(\varepsilon) \varepsilon d\varepsilon = \int_{-1}^{1} y_i(x) m(xb) x dx \tag{127}$$

The elastic and damping moments are

$$M_E = -K_\alpha \alpha(t) \tag{128}$$

$$M_D = -C_\alpha \dot{\alpha}(t), \tag{129}$$

and the external moment, the aerodynamic moment, M, is given by Equation (48) with $\dot{X} = \ddot{X} = 0$, or with the heave (Y) and pitching (α) motion explicitly included in the formulation, Equation (B.4) in Appendix B. As in the case of the normal force, the moments should be in equilibrium with each other

$$\begin{aligned} M_I + M_E + M_D + M &= 0 \\ &\Updownarrow \\ M_{tot}(ab-\varepsilon_{cg})\ddot{Y} + I_a\ddot{\alpha} + C_\alpha\dot{\alpha} + K_\alpha\alpha - M_{fict} - M &= 0 \end{aligned} \tag{130}$$

where the moment due to the deformation of the airfoil, M_{fict}, is

$$M_{fict} = abN_{fict} + b^2 \sum_{i=1}^{Ndefl} D\ddot{e}fl_i Ims_i \tag{131}$$

Deformation motion equations

The differential equation governing the deformation of the airfoil is

$$\frac{\partial^2}{\partial \varepsilon^2}\left[EI\frac{\partial^2 y}{\partial \varepsilon^2} + c_s I \frac{\partial^3 y}{\partial \varepsilon^2 \partial t}\right] + m\frac{\partial^2 y}{\partial t^2} + c\frac{\partial y}{\partial t} = \Delta P(\varepsilon/b) + P_{fict} \tag{132}$$

The local aerodynamic force, $\Delta P(\varepsilon/b)$, is given in Equation (51) (or the version with the heave and pitching motions stated explicitly, Equation (B.5), in the Appendix B). P_{fict}

is the local fictitious inertia force from the acceleration of the airfoil coordinate system. The acceleration of the airfoil coordinate system is

$$\begin{aligned} Y^*(\varepsilon,t) &= Y(t) + (ab-\varepsilon)\alpha(t) \\ &\Updownarrow \\ \ddot{Y}^*(\varepsilon,t) &= \ddot{Y}(t) + (ab-\varepsilon)\ddot{\alpha}(t), \end{aligned} \tag{133}$$

which leads to

$$P_{fict} = -\ddot{Y}^*(\varepsilon,t)m(\varepsilon) = -\left(\ddot{Y}(t) + (ab-\varepsilon)\ddot{\alpha}(t)\right) m(\varepsilon), \tag{134}$$

The free vibrational modes, y_i, and corresponding eigenfrequencies, ω_i, are determined from the eigenvalue problem

$$\frac{\partial^2}{\partial\varepsilon^2}\left[EI\frac{\partial^2 y_i}{\partial\varepsilon^2}\right] - \omega_i^2 m y_i = 0. \tag{135}$$

Using the free vibration modes, y_i, of the elastic airfoil clamped at $\varepsilon = ab$, the equation of motion for the deformation of the airfoil, Equation (130), is formulated in terms of the free vibration modes with the modal amplitude functions, $Defl_i$, as generalized coordinates, i.e. using the modal decomposition in Equation (111). The vibrational modes are orthogonal, meaning that

$$\int_{-b}^{b} y_i m y_j d\varepsilon = m_i \delta_{i,j}, \tag{136}$$

where m_i are modal masses, and $\delta_{i,j}$ is the Kronecker delta. By introducing the modal decomposition, Equation (111), into the differential equation governing the deformation of the airfoil, Equation (132), and integrating the result multiplied by y_i over the airfoil, we obtain with the aid of Equation (136), Equation (135) and the assumption of orthogonal damping

$$m_i \ddot{Defl_i} + m_i 2\omega_i \xi_s \dot{Defl_i} + m_i \omega_i^2 Defl_i - MF_i - \int_{-b}^{b} y_i \Delta P(\varepsilon/b) dx = 0 \tag{137}$$

In Equation (137), ξ_s is the structural damping ratio, and MF_i are the fictitious modal forces from the heave and pitching acceleration, given by

$$\begin{aligned} MF_i &= \int_{-b}^{b} y_i P_{fict} d\varepsilon \\ &= -\int_{-b}^{b} y_i(\varepsilon/b)\left(\ddot{Y} + (ab-\varepsilon)\ddot{\alpha}\right) m(\varepsilon) d\varepsilon \\ &= -b(\ddot{Y} + ab\ddot{\alpha}) Ins_i + \ddot{\alpha} b^2 Ims_i \end{aligned} \tag{138}$$

The integral over the fluid forces is somewhat more elaborate, but quite straightforward. The deflection shape integrals in the expression turns out to be identical to those in the equations for the power, Equations (68) or (B.7) in the appendix. The result is

$$\begin{aligned} \int_{-b}^{b} y_i \Delta P(\varepsilon/b) dx &= 2\rho\left(-\ddot{X}\alpha + (V-\dot{X})\dot{\alpha} - \ddot{Y} - ab\ddot{\alpha}\right) PI1_i \\ &\quad + \rho b \frac{1}{\pi}\Bigg(\sum_{j=1}^{Ndefl} \ddot{Defl_j}(t) PI2_{i,j} \\ &\quad - \ddot{X}(t) \sum_{j=1}^{Ndefl} Defl_j(t) PI3_{i,j} \end{aligned}$$

$$
\begin{aligned}
&+(V-\dot{X}(t))\sum_{j=1}^{Ndefl}\dot{Defl}_j(t)PI3_{i,j}\Bigg)\\
&+\rho b^2\ddot{\alpha}PI4_i-2\rho(V-\dot{X}(t))Q\mathbf{C}PI5_i\\
&-2\rho(V-\dot{X}(t))\Bigg(\frac{b}{2}\,\dot{\alpha}PI6_i\\
&\qquad+\frac{(V-\dot{X}(t))}{2\pi}\sum_{j=1}^{Ndefl}Defl_j(t)H_{dyd\varepsilon,j}PI7_i\\
&\qquad-\frac{(V-\dot{X}(t))}{2\pi}\sum_{j=1}^{Ndefl}Defl_j(t)PI8_{i,j}\\
&\qquad+\frac{1}{2\pi}\sum_{j=1}^{Ndefl}\dot{Defl}_j(t)H_{y,j}PI7_i\\
&\qquad-\frac{1}{2\pi}\sum_{j=1}^{Ndefl}\dot{Defl}_j(t)PI9_{i,j}\Bigg)
\end{aligned}
\tag{139}
$$

Determination of stability

Since the equations for the motion of the airfoil in the heaving (Equation (123)) and pitching directions (Equation (130)), the deformation of the airfoil (Equation (137)), and the equations for the aerodynamic state variables (Equation (83)), are all linear for $\dot{X} = \ddot{X} = 0$ it is possible to express the full linear system as a matrix equation

$$
\underline{\underline{\mathbf{M}}}\,\underline{\ddot{\mathbf{d}}}+\underline{\underline{\mathbf{C}}}\,\underline{\dot{\mathbf{d}}}+\underline{\underline{\mathbf{K}}}\,\underline{\mathbf{d}} \quad = \quad \underline{\mathbf{0}} \tag{140}
$$

where $\underline{\mathbf{d}} = [Y;\alpha;Defl_1;...Defl_{Ndefl};z_1;...z_{Naero}]^T$. Since the aerodynamic state variables z_i are not dependent on any second order derivatives of time, Equation (140) can be rewritten to a first order matrix equation

$$
\underline{\dot{\tilde{\mathbf{d}}}} \quad = \quad \underline{\underline{\mathbf{A}}}\,\underline{\tilde{\mathbf{d}}} \tag{141}
$$

where $\underline{\tilde{\mathbf{d}}} = [\dot{Y};\dot{\alpha};\dot{Defl}_1;...\dot{Defl}_{Ndefl};Y;\alpha;Defl_1;...Defl_{Ndefl};z_1;...z_{Naero}]^T$. The stability of the system is determined by inserting the solution

$$
\underline{\tilde{\mathbf{d}}} \quad = \quad \underline{\widehat{\mathbf{d}}}e^{\lambda t} \tag{142}
$$

into Equation (141). This yields

$$
\left(\underline{\underline{\mathbf{A}}}-\lambda\underline{\underline{\mathbf{I}}}\right)\underline{\widehat{\mathbf{d}}}e^{\lambda t} \quad = \quad \underline{\mathbf{0}} \tag{143}
$$

The nontrivial solution to this problem is

$$
det\left(\underline{\underline{\mathbf{A}}}-\lambda\underline{\underline{\mathbf{I}}}\right) \quad = \quad 0, \tag{144}
$$

which is a polynomium in the complex variable λ. This can be solved using any standard eigenvalue problem solver, and the solutions in λ are called eigenvalues. From Equation (142) it is seen that the system is stable if the greatest real part of the eigenvalues is negative.

Computational example

Consider an airfoil with constant camberline bending stiffness EI and constant distributed mass, $m = M_{tot}/(2b)$. The moment of inertia around a point $\varepsilon = ab$ of the stiff airfoil is $I_a = M_{tot}b^2(1/3+a^2)$. The undamped vibration modes and frequencies of an

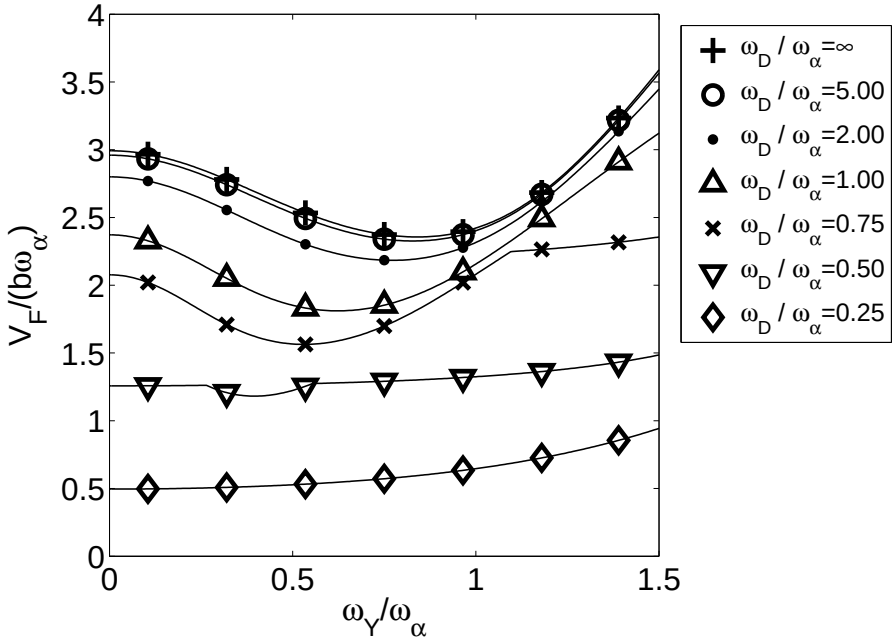

Figure 6: *Non-dimensional flutter limits for airfoil of different uniform chordwise stiffness as function of the undamped heave to pitch frequency ratio.* ω_D *is the lowest eigenfrequency of the undamped elastic airfoil clamped at* $\varepsilon = ab$*. The nondimensional elastic hinge point is* $a = -0.4$*.*

elastic 2D plate clamped at $\varepsilon = ab$ consists of uniform cantilever beam vibration modes and frequencies for each end, $-b$ to ab and ab to b. The modal vibration frequencies of an uniform cantilever beam of length l are found by solving the transendental equation

$$\cos(l\sqrt{\omega/a}) \quad = \quad -\frac{1}{\cosh(l\sqrt{\omega/a})}. \tag{145}$$

where $a^2 = EI/m$. The corresponding vibrational modes are found by inserting the found frequencies, $\omega_1, \omega_2, \ldots \omega_n$ into

$$\begin{aligned}\hat{y}_i(\tilde{x}) \quad = \quad & \frac{\sin(l\sqrt{\omega_i/a}) - \sinh(l\sqrt{\omega_i/a})}{\cos(l\sqrt{\omega_i/a}) + \cosh(l\sqrt{\omega_i/a})}\left(\sinh(\tilde{x}\sqrt{\omega_i/a}) - \sin(\tilde{x}\sqrt{\omega_i/a})\right) \\ & + \left(\cosh(\tilde{x}\sqrt{\omega_i/a}) - \cos(\tilde{x}\sqrt{\omega_i/a})\right). \end{aligned} \tag{146}$$

where $\tilde{x}$ is a length parameter, going from zero at the clamped position to l at the free end.

Figure 6 show the non-dimensional flutter limits versus structural frequency ratios ω_Y/ω_α for elastically hinged 2D airfoils of different camberline stiffness. For flow velocities below the flutter limit, V_F, oscillations are damped out, whereas they are increased for flow velocities above V_F. The non-dimensional hinge point is $a = -0.4$, and the mass ratio is $M_{tot}/(\pi\rho b^2) = 20$. The chordwise stiffness is expressed non-dimensionally in terms of the frequency ratio ω_D/ω_α, where ω_D is the lowest eigenfrequency of the undamped elastic airfoil clamped at $\varepsilon = ab$, which in this case is the lowest eigenfrequency of the downwind end of length $b - ab$. The results in the figure are computed using two upwind and three downwind vibration modes. The results using one upwind and two downwind deflection mode shapes are only marginally different from the ones with the finer resolution. The maximum absolute difference in non-dimensional flutter velocity is below 0.02 and the mean absolute change is below 0.0025.

As expected, Figure 6 show that the flutter velocities tend to the classical flutter results as

the stiffness is increased, $\omega_D \to \infty$. Furthermore, it is seen that flutter velocities decrease as the airfoil stiffness is decreased. The airfoils used in both aeronautical and wind energy applications have chordwise deformations with very high eigenfrequencies compared to the eigenfrequency of the pitching motion, so the ordinary rigid theory is fully adequate in those cases. However, for applications within soft propulsors for hydrodynamic devices, camberline elasticity may change the flutter velocity considerably compared to classic rigid airfoil theory.

5 Conclusions

In the present report analytical expressions for distributed and integral unsteady 2D forces on a variable geometry thin airfoil undergoing arbitrary motion were derived under the assumption of incompressible, irrotational, inviscid flow. It was shown from the expressions for the forces, that the influence from the shed vorticity in the wake is described by the same time-lag for all chordwise positions on the airfoil. This time-lag term was approximated using an indicial function approach, allowing for numerically very efficient computation of the aerodynamic response by use of Duhamel superposition. Furthermore, the indicial function expressions for the time-lag terms were formulated in their equivalent state-space form, allowing for use of the present theory in problems employing the eigenvalue approach, such as stability analysis.

The analytical expressions for the forces simplify to the thin-airfoil results by Munk [18] in case of steady flow, and Theodorsen [20] in case of unsteady flow over a flat airfoil with a flat flap. Comparisons of the thrust predicted with the present algorithm is in excellent agreement with the analytical results of Garrick [7] and Wu [22] for a heaving flat plate and a progressing wave of given wavelength and phase velocity over the chord, respectively. Furthermore, it was shown how the present theory could be used to predict an arbitrary forcing from vertical gusts, and this method was verified by comparison with Sears function [19].

The current theory can be used for various applications which up to now have been possible only using much more computational costly methods. The propulsive performance of a soft heaving propulsor, and the influence of airfoil camberline elasticity on the flutter limit are two computational examples given in the report that highlight this feature. The conclusions from the computations on the soft heaving propulsor computations agree with classical results: thrust decrease, and propulsive efficiency increase as the propulsor stiffness is decreased. The results from the predictions of the influence of airfoil camberline elasticity on the flutter limit show that the ordinary rigid airfoil theory is fully adequate for the airfoils on aeroplanes and wind turbines.

Acknowledgement

The author gratefully acknowledges that this work was partly funded under the Danish Research Council under the ADAPWING project.

References

[1] Andersen, P.B. *Load Alleviation on Wind Turbine Blades using Variable Airfoil Geometry (2D and 3D study)* M.Sc. Thesis, Technical University of Denmark, Department of Mechanical Engineering, Section of Fluid Mechanics. June 2005.

[2] Bossanyi, E.A *Individual Blade Pitch Control for Load Reduction.* Wind Energy 6 (2), April-June 2003. p. 119-128

[3] Bossanyi, E.A *Wind Turbine Control for Load Reduction.* Wind Energy 6 (3), July-September 2003. p. 229-244

[4] Bossanyi, E.A *Further Load Reductions with Individual Pitch Control.* Wind Energy 8 (4), October-December 2005. p. 481-485.

[5] Buhl, T., Gaunaa, M. & Bak, C. *Potential Load Reduction Using Airfoils with Variable Trailing Edge Geometry.* Journal of Solar Energy Eng., Vol. 127, November 2005. p. 503-516

[6] von Karman, T. & Burgers, J.M. *Aerodynamic Theory: A General Review of Progress. Vol II. General Aerodynamic Theory, Perfect Fluids.* Editor W.F. Durand. Julius Springer, 1935.

[7] Garrick, I.E. *Propulsion of a Flapping and Oscillating Airfoil.* NACA Report No. 567. 1936.

[8] Gaunaa, M. *Unsteady Aerodynamic Forces on NACA 0015 Airfoil in Harmonic Translatory Motion.* Ph.D. Thesis. Fluid Mechanics, Department of Mechanical Engineering, Technical University of Denmark, April 2002.

[9] Glauert, H. *The Force and Moment on an Oscillating Aerofoil.* Tech. Rep. Aero. Res. Comm. 1242, 1929.

[10] Hansen, M.H., Gaunaa, M. & Madsen, H.Aa. *A Beddoes-Leishman Type Dynamic Stall Model in State-Space and Indicial Formulations.* Technical report - Risø-R-1354(EN). June 2004.

[11] Hariharan, N. & Leishman, J.G. *Unsteady Aerodynamics of a Flapped Airfoil in Subsonic Flow by Indicial Concepts.* Journal of Aircraft, Vol. 33(5), 1996. p. 855-868.

[12] Jones, R.T. *The Unsteady Lift of a Wing of Finite Aspect Ratio.* NACA Report 681. 1939.

[13] von Karman, Th. & Sears, W.R. *Airfoil Theory for Non-Uniform Motion.* Journal of the Aeronautical Sciences. 5(10) 1938. p.379-390

[14] Katz, J. & Weihs, D. *Hydrodynamic Propulsion by Large Amplitude Oscillation of an Airfoil With Chordwise Flexibility.* J. Fluid Mech. 1978. 88(3). p.485-497.

[15] Katz, J. & Weihs, D. *The Effect of Chordwise Flexibility on the Lift of a Rapidly Accelerated Airfoil.* Aeronautical Quarterly. 1979. 30. p.360-370.

[16] Larsen, T.J., Madsen, H.Aa. & Thomsen, K. *Active Load Reduction Using Individual Pitch, Based on Local Blade Flow Measurements.* Wind Energy, 8(1). January-March 2005. p.67-80.

[17] Leishman, J.G. *Unsteady Lift of a Flapped Airfoil by Indicial Concepts.* Journal of Aircraft, Vol. 31(2), 1994, p. 288-297.

[18] Munk, M. *General Theory of Thin Wing Sections.* NACA Report 142. 1922.

[19] Sears, W.R. *Some Aspects of Non-Stationary Airfoil Theory and Its Practical Application.* Journal of the Aeronautical Sciences. 8(3) 1941. p.104-108

[20] Theodorsen, T. *General Theory of Aerodynamical Instability and the Mechanism of Flutter.* NACA Report 496. 1935.

[21] van der Wall, B.G., & Geissler,W. *Experimental and Numerical Investigations on Steady and Unsteady Behaviour of a Rotor Airfoil with a Piezoelectric Trailing Edge Flap*. 55th American Helicopter Society Forum, Montreal, Canada. May 1999.

[22] Wu, T.Y. *Swimming of a wawing plate.* J. Fluid Mech. 1961. 10(3). p.321-324

[23] Wu, T.Y. *Hydromechanics of Swimming Propulsion. Pt. 1. Swimming of a Two-Dimensional Flexible Plate at Variable Forward Speeds in an Inviscid Fluid* J. Fluid Mech. 1971. 46(2). p.337-355

A General Surface Velocity Potential

The resulting velocity potential of a source of strength dS in the complex plane at $\xi = \xi_{1s} + i \cdot \xi_{2s}$ and a source of opposite strength (drain) $-dS$ at $\xi = \xi_{1s} - i \cdot \xi_{2s}$ is

$$\varphi_{sd\xi}(\xi, \xi_s) = \frac{dS}{4\pi} \ln \left(\frac{(\xi_1 - \xi_{1s})^2 + (\xi_2 - \xi_{2s})^2}{(\xi_1 - \xi_{1s})^2 + (\xi_2 + \xi_{2s})^2} \right) \tag{A.1}$$

Placing the source/drain pair on a circle of radius $b/2$ with centrum in $\xi = 0$ in the ξ plane, and considering only points on the same circle, the result is

$$\xi_2 = \sqrt{b^2/4 - \xi_1} \tag{A.2}$$

$$\xi_{2s} = \sqrt{b^2/4 - \xi_{1s}}, \tag{A.3}$$

which inserted into (A.1) yield the surface velocity potential of the source/drain pair in the ξ plane

$$\varphi_{sd\xi}(\xi_1, \xi_{1s}) = \frac{dS}{4\pi} \ln \left(\frac{(\xi_1 - \xi_{1s})^2 + \left(\sqrt{b^2/4 - \xi_1} - \sqrt{b^2/4 - \xi_{1s}}\right)^2}{(\xi_1 - \xi_{1s})^2 + \left(\sqrt{b^2/4 - \xi_1} + \sqrt{b^2/4 - \xi_{1s}}\right)^2} \right) \tag{A.4}$$

The well known Joukowski transformation

$$z = \xi + \frac{b^2}{4\,\xi} \tag{A.5}$$

maps the circle $\xi = \xi_1 + i \cdot \sqrt{b^2/4 - \xi_1^2}$, $-b/2 \leq \xi_1 \leq b/2$ onto the real axis in the z plane $z = z_1 + i \cdot z_2 = 2\xi_1 + i \cdot 0$. Therefore, the surface velocity potential in the z-plane is obtained by inserting $\xi_1 = 1/2\, z_1$ and $\xi_{1s} = 1/2\, z_{1s}$ into Equation (A.4)

$$\varphi_{sdz}(z_1, z_{1s}) = \frac{dS}{4\pi} \ln \left(\frac{(z_1 - z_{1s})^2 + \left(\sqrt{b^2 - z_1} - \sqrt{b^2 - z_{1s}}\right)^2}{(z_1 - z_{1s})^2 + \left(\sqrt{b^2 - z_1} + \sqrt{b^2 - z_{1s}}\right)^2} \right) \tag{A.6}$$

Converting the from dimensional to non-dimensional coordinates by insertion of $xb = z_1$ and $x_1 b = z_{1s}$ yield

$$\varphi_{sd}(x, x_1) = \frac{dS}{4\pi} \ln \left(\frac{(x - x_1)^2 + \left(\sqrt{b^2 - x} - \sqrt{b^2 - x_1}\right)^2}{(x - x_1)^2 + \left(\sqrt{b^2 - x} + \sqrt{b^2 - x_1}\right)^2} \right) \tag{A.7}$$

The surface velocity potential of a distributed sheet of sources with strength $\sigma(x_1, t)$ on the upper side of the airfoil, and a distributed sheet of sources of the opposite strength ($-\sigma(x_1, t)$) on the lower side of the airfoil can be obtained by integration. Since

$$dS\,|_{x=x_1} = \sigma(x_1, t) b\; dx_1 \tag{A.8}$$

the surface velocity potential is obtained by integration

$$\varphi(x, t) = \frac{b}{4\pi} \int_{-1}^{1} \sigma(x_1, t) \ln \left(\frac{(x - x_1)^2 + \left(\sqrt{1 - x^2} - \sqrt{1 - {x_1}^2}\right)^2}{(x - x_1)^2 + \left(\sqrt{1 - x^2} + \sqrt{1 - {x_1}^2}\right)^2} \right) dx_1 \tag{A.9}$$

B Full Force Expressions

For airfoil computations it may sometimes be convenient to have the expressions for the forces on the airfoil with the heaving and pitching deflection mode explicitly given. For heaving motion, the deformation mode shape is $y_Y(x) = 1$ and the derivative is $\partial y_Y(x)/\partial\varepsilon = 0$, and for pitching motion with non-dimensional center of rotation at $x = a$ the deformation mode shape is $y_\alpha(x) = b(a - x)$ and the derivative $\partial y_\alpha(x)/\partial\varepsilon = -1$. Upon inserting the velocity potentials corresponding to these deformation shapes, listed in Appendix D, the full force expressions, including the heave and pitch degrees of freedom explicitly, can be stated. Note that in this case, the normal and tangential forces, N and T, are the forces in the direction normal and tangential (positive from trailing edge to leading edge) to the airfoil coordinate system: that is, it is rotated the angle α (in the clockwise direction) compared to the normal and tangential force in the general formulation given in the main report, Equations (45) and (59).

$$
\begin{aligned}
N_c(c) &= \rho b^2 K_1(c)\left(-\ddot{X}\alpha + (V-\dot{X})\dot{\alpha} - \ddot{Y} - ab\ddot{\alpha}\right) \\
&+ \frac{\rho\, b^2}{\pi}\Bigg(\sum_{i=1}^{Ndefl} D\ddot{e}fl_i(t)F_{y,i}(c) - \ddot{X}(t)\sum_{i=1}^{Ndefl} Defl_i(t)F_{dyd\varepsilon,i}(c) \\
&\qquad + \left(V-\dot{X}(t)\right)\sum_{i=1}^{Ndefl} D\dot{e}fl_i(t)F_{dyd\varepsilon,i}(c)\Bigg) \\
&+ \rho b^3 K_2(c)\ddot{\alpha} \\
&+ 2\,b\rho\left(V-\dot{X}(t)\right)\left(\arccos(c) - \sqrt{1-c^2}\right)Q\mathbf{C} \\
&- b\rho\sqrt{1-c^2}\left(V-\dot{X}(t)\right)\Bigg(\frac{\left(V-\dot{X}(t)\right)\sum_{i=1}^{Ndefl} Defl_i(t)H_{dyd\varepsilon,i}}{\pi} \\
&\qquad + \frac{\sum_{i=1}^{Ndefl} D\dot{e}fl_i(t)H_{y,i}}{\pi} - b(1-c)\dot{\alpha}\Bigg) \\
&- \rho\, b\left(V-\dot{X}(t)\right)\Bigg(\frac{\left(V-\dot{X}(t)\right)\sum_{i=1}^{Ndefl} Defl_i(t)f_{dyd\varepsilon,i}(c)}{\pi} \\
&\qquad + \frac{\sum_{i=1}^{Ndefl} D\dot{e}fl_i(t)f_{y,i}(c)}{\pi}\Bigg)
\end{aligned}
\tag{B.1}
$$

$$
\begin{aligned}
N &= \rho b^2\pi\left(-\ddot{X}\alpha + (V-\dot{X})\dot{\alpha} - \ddot{Y} - ab\ddot{\alpha}\right) \\
&+ \frac{\rho b^2}{\pi}\sum_{i=1}^{Ndefl}\Bigg(D\ddot{e}fl_i(t)F_{y,i}(-1) - \ddot{X}Defl_i(t)F_{dyd\varepsilon,i}(-1) \\
&\qquad + (V-\dot{X})D\dot{e}fl_i(t)F_{dyd\varepsilon,i}(-1)\Bigg) \\
&+ 2\pi\rho b(V-\dot{X})\cdot Q\mathbf{C}
\end{aligned}
\tag{B.2}
$$

$$
\begin{aligned}
M_c(c) &= \rho\left((-ac-1/8)K_1(c) + 2(a+c/8)K_2(c)\right)b^4\ddot{\alpha} \\
&\quad + \rho\left((c-1/2)K_1(c) - K_2(c)\right)(V-\dot{X})b^3\dot{\alpha}
\end{aligned}
$$

$$
\begin{aligned}
&+\rho b^3(-K_1(c)\,c+2K_2(c))\ddot{X}\alpha+\rho b^3(-K_1(c)\,c+2K_2(c))\ddot{Y}\\
&+\rho b^3\frac{1}{\pi}\ddot{X}(t)\sum_{i=1}^{Ndefl}Defl_i(t)\,(G_{dyd\varepsilon,i}(c)-cF_{dyd\varepsilon,i}(c))\\
&+\rho b^2\frac{1}{\pi}(V-\dot{X}(t))^2\sum_{i=1}^{Ndefl}Defl_i(t)F_{dyd\varepsilon,i}(c)\\
&+\rho b^2(V-\dot{X}(t))^2\frac{K_1(c)}{2\pi}\sum_{i=1}^{Ndefl}Defl_iH_{dyd\varepsilon,i}\\
&-\rho b^3\frac{1}{\pi}(V-\dot{X}(t))\sum_{i=1}^{Ndefl}D\dot{e}fl_i(t)(G_{dyd\varepsilon,i}(c)-cF_{dyd\varepsilon,i}(c))\\
&+\rho b^2\frac{1}{\pi}(V-\dot{X}(t))\sum_{i=1}^{Ndefl}D\dot{e}fl_i(t)F_{y,i}(c)\\
&+\rho b^2(V-\dot{X}(t))\frac{K_1(c)}{2\pi}\sum_{i=1}^{Ndefl}D\dot{e}fl_i(t)H_{y,i}\\
&-\rho b^3\frac{1}{\pi}\sum_{i=1}^{Ndefl}D\ddot{e}fl_i(t)(G_{y,i}(c)-cF_{y,i}(c)) \qquad \text{(B.3)}\\
&+2\rho b^2(V-\dot{X}(t))\left((c+1/2)\arccos(c)-(1+c/2)\sqrt{1-c^2}\right)Q\mathbf{C}
\end{aligned}
$$

$$
\begin{aligned}
M \;=\;& \rho\pi(-1/8-a^2)b^4\ddot{\alpha}-\pi b^3\rho(V-\dot{X})(1/2-a)\dot{\alpha}-\rho\pi b^3a\ddot{X}\alpha-\rho\pi ab^3\ddot{Y}\\
&+\rho b^3\frac{1}{\pi}\ddot{X}(t)\sum_{i=1}^{Ndefl}Defl_i(t)\,(G_{dyd\varepsilon,i}(-1)-aF_{dyd\varepsilon,i}(-1))\\
&+\rho b^2\frac{1}{\pi}(V-\dot{X}(t))^2\sum_{i=1}^{Ndefl}Defl_i(t)F_{dyd\varepsilon,i}(-1)\\
&+\rho b^2(V-\dot{X}(t))^2\frac{1}{2}\sum_{i=1}^{Ndefl}Defl_iH_{dyd\varepsilon,i}\\
&-\rho b^3\frac{1}{\pi}(V-\dot{X}(t))\sum_{i=1}^{Ndefl}D\dot{e}fl_i(t)(G_{dyd\varepsilon,i}(-1)-aF_{dyd\varepsilon,i}(-1))\\
&+\rho b^2\frac{1}{\pi}(V-\dot{X}(t))\sum_{i=1}^{Ndefl}D\dot{e}fl_i(t)F_{y,i}(-1)\\
&+\rho b^2(V-\dot{X}(t))\frac{1}{2}\sum_{i=1}^{Ndefl}D\dot{e}fl_i(t)H_{y,i}\\
&-\rho b^3\frac{1}{\pi}\sum_{i=1}^{Ndefl}D\ddot{e}fl_i(t)(G_{y,i}(-1)-aF_{y,i}(-1)) \qquad \text{(B.4)}\\
&+2\pi\rho b^2(V-\dot{X}(t))(1/2+a)Q\mathbf{C}
\end{aligned}
$$

$$
\Delta P(c) \;=\; \rho b2\sqrt{1-c^2}\left(-\ddot{X}\alpha+(V-\dot{X})\dot{\alpha}-\ddot{Y}-ab\ddot{\alpha}\right)
$$

$$
\begin{aligned}
&+\rho b^2 c\sqrt{1-c^2}\ddot{\alpha} - \rho b(V-\dot{X})\frac{(2c+1)(c-1)}{\sqrt{1-c^2}}\,\dot{\alpha} \\
&+\rho b\frac{1}{\pi}\Bigg(\sum_{i=1}^{Ndefl} D\ddot{e}fl_i(t)f_{y,i}(c) \\
&\qquad -\ddot{X}(t)\sum_{i=1}^{Ndefl} Defl_i(t)f_{dyd\varepsilon,i}(c) \\
&\qquad +(V-\dot{X}(t))\sum_{i=1}^{Ndefl} D\dot{e}fl_i(t)f_{dyd\varepsilon,i}(c)\Bigg) \\
&-2\rho(V-\dot{X}(t))\frac{c-1}{\sqrt{1-c^2}}Q\mathbf{C} \\
&-\rho\frac{1}{\pi}(V-\dot{X}(t))^2\Bigg(\frac{c}{\sqrt{1-c^2}}\sum_{i=1}^{Ndefl} Defl_i(t)H_{dyd\varepsilon,i} \\
&\qquad -\sum_{i=1}^{Ndefl} Defl_i(t)\frac{\partial f_{dyd\varepsilon,i}(c)}{\partial c}\Bigg) \\
&-\rho\frac{1}{\pi}(V-\dot{X}(t))\Bigg(\frac{c}{\sqrt{1-c^2}}\sum_{i=1}^{Ndefl} D\dot{e}fl_i(t)H_{y,i} \\
&\qquad -\sum_{i=1}^{Ndefl} D\dot{e}fl_i(t)\frac{\partial f_{y,i}(c)}{\partial c}\Bigg)
\end{aligned}
\tag{B.5}
$$

$$
\begin{aligned}
T \;=\; & \frac{\pi}{2}\rho b\Bigg(2Q\mathbf{C} - \dot{\alpha}b + \frac{V-\dot{X}(t)}{2\pi}\sum_{i=1}^{Ndefl} Defl_i(t)(K_{dyd\varepsilon,i}+H_{dyd\varepsilon,i}) \\
&\qquad +\frac{1}{2\pi}\sum_{i=1}^{Ndefl} D\dot{e}fl_i(t)(K_{y,i}+H_{y,i})\Bigg)^2 \\
&+2\rho b^2\left(-\ddot{X}\alpha + (V-\dot{X})\dot{\alpha} - \ddot{Y} - ab\ddot{\alpha}\right)\sum_{i=1}^{Ndefl} Defl_i(t)TI1_i \\
&+\rho b^2\frac{1}{\pi}\Bigg(\sum_{i=1}^{Ndefl}\sum_{j=1}^{Ndefl} Defl_i(t)D\ddot{e}fl_j(t)TI2_{i,j} \\
&\qquad -\ddot{X}(t)\sum_{i=1}^{Ndefl}\sum_{j=1}^{Ndefl} Defl_i(t)Defl_j(t)TI3_{i,j} \\
&\qquad +(V-\dot{X}(t))\sum_{i=1}^{Ndefl}\sum_{j=1}^{Ndefl} Defl_i(t)D\dot{e}fl_j(t)TI3_{i,j}\Bigg) \\
&+\rho b^3\ddot{\alpha}\sum_{i=1}^{Ndefl} Defl_i(t)TI4_i - 2b\rho(V-\dot{X}(t))Q\mathbf{C}\sum_{i=1}^{Ndefl} Defl_i(t)TI5_i \\
&-2\rho b(V-\dot{X}(t))\Bigg(\frac{b}{2}\,\dot{\alpha}\sum_{i=1}^{Ndefl} Defl_i(t)TI6_i \\
&\qquad +\frac{(V-\dot{X}(t))}{2\pi}\sum_{i=1}^{Ndefl}\sum_{j=1}^{Ndefl} Defl_i(t)Defl_j(t)H_{dyd\varepsilon,j}TI7_i
\end{aligned}
$$

$$
\begin{aligned}
&-\frac{(V-\dot{X}(t))}{2\pi}\sum_{i=1}^{Ndefl}\sum_{j=1}^{Ndefl} Defl_i(t)Defl_j(t)TI8_{i,j} \\
&+\frac{1}{2\pi}\sum_{i=1}^{Ndefl}\sum_{j=1}^{Ndefl} Defl_i(t)D\dot{e}fl_j(t)H_{y,j}TI7_i \\
&-\frac{1}{2\pi}\sum_{i=1}^{Ndefl}\sum_{j=1}^{Ndefl} Defl_i(t)D\dot{e}fl_j(t)TI9_{i,j}\Bigg)
\end{aligned} \tag{B.6}
$$

$$
\begin{aligned}
Pow \;=\; & -2\rho b^2\left(-\ddot{X}\alpha+(V-\dot{X})\dot{\alpha}-\ddot{Y}-ab\ddot{\alpha}\right)\sum_{i=1}^{Ndefl} D\dot{e}fl_i(t)PI1_i \\
&-\rho b^2\frac{1}{\pi}\Bigg(\sum_{i=1}^{Ndefl}\sum_{j=1}^{Ndefl} D\dot{e}fl_i(t)D\ddot{e}fl_j(t)PI2_{i,j} \\
&\qquad -\ddot{X}(t)\sum_{i=1}^{Ndefl}\sum_{j=1}^{Ndefl} D\dot{e}fl_i(t)Defl_j(t)PI3_{i,j} \\
&\qquad +(V-\dot{X}(t))\sum_{i=1}^{Ndefl}\sum_{j=1}^{Ndefl} D\dot{e}fl_i(t)D\dot{e}fl_j(t)PI3_{i,j}\Bigg) \\
&-\rho b^3\ddot{\alpha}\sum_{i=1}^{Ndefl} D\dot{e}fl_i(t)PI4_i+2b\rho(V-\dot{X}(t))Q\mathbf{C}\sum_{i=1}^{Ndefl} D\dot{e}fl_i(t)PI5_i \\
&+2\rho b(V-\dot{X}(t))\Bigg(\frac{b}{2}\,\dot{\alpha}\sum_{i=1}^{Ndefl} D\dot{e}fl_i(t)PI6_i \\
&\qquad +\frac{(V-\dot{X}(t))}{2\pi}\sum_{i=1}^{Ndefl}\sum_{j=1}^{Ndefl} D\dot{e}fl_i(t)Defl_j(t)H_{dyd\varepsilon,j}PI7_i \\
&\qquad -\frac{(V-\dot{X}(t))}{2\pi}\sum_{i=1}^{Ndefl}\sum_{j=1}^{Ndefl} D\dot{e}fl_i(t)Defl_j(t)PI8_{i,j} \\
&\qquad +\frac{1}{2\pi}\sum_{i=1}^{Ndefl}\sum_{j=1}^{Ndefl} D\dot{e}fl_i(t)D\dot{e}fl_j(t)H_{y,j}PI7_i \\
&\qquad -\frac{1}{2\pi}\sum_{i=1}^{Ndefl}\sum_{j=1}^{Ndefl} D\dot{e}fl_i(t)D\dot{e}fl_j(t)PI9_{i,j}\Bigg) \\
&-N\dot{Y}-M\dot{\alpha}
\end{aligned} \tag{B.7}
$$

The equivalent flat plate three-quarter downwash is in the full explicit case

$$
\begin{aligned}
Q \;=\; & (V-\dot{X})\alpha-\dot{Y}+(1/2-a)b\dot{\alpha} \\
&-\frac{1}{2\pi}\left(V-\dot{X}(t)\right)\sum_{i=1}^{Ndefl} Defl_i(t)H_{dyd\varepsilon,i} \\
&-\frac{1}{2\pi}\sum_{i=1}^{Ndefl} D\dot{e}fl_i(t)H_{y,i}
\end{aligned} \tag{B.8}
$$

The constants and deflection shape integrals in the force expressions are listed below

$$
K_1(c) \;=\; \pi/2-c\sqrt{1-c^2}-\arcsin c=\arccos(c)-c\sqrt{1-c^2} \tag{B.9}
$$

$$K_2(c) = 1/3(1-c^2)^{3/2} \tag{B.10}$$

$$f_{y,i}(x) = \int_{-1}^{1} y_i(x_1) \ln\left(\frac{(x-x_1)^2 + \left(\sqrt{1-x^2} - \sqrt{1-{x_1}^2}\right)^2}{(x-x_1)^2 + \left(\sqrt{1-x^2} + \sqrt{1-{x_1}^2}\right)^2}\right) dx_1 \tag{B.11}$$

$$f_{dyd\varepsilon,i}(x) = \int_{-1}^{1} y_i'(x_1) \ln\left(\frac{(x-x_1)^2 + \left(\sqrt{1-x^2} - \sqrt{1-{x_1}^2}\right)^2}{(x-x_1)^2 + \left(\sqrt{1-x^2} + \sqrt{1-{x_1}^2}\right)^2}\right) dx_1 \tag{B.12}$$

$$F_{y,i}(c) = \int_{c}^{1} f_{y,i}(x)dx \tag{B.13}$$

$$G_{y,i}(c) = \int_{c}^{1} x f_{y,i}(x)dx \tag{B.14}$$

$$F_{dyd\varepsilon,i}(c) = \int_{c}^{1} f_{dyd\varepsilon,i}(x)dx \tag{B.15}$$

$$G_{dyd\varepsilon,i}(c) = \int_{c}^{1} x f_{dyd\varepsilon,i}(x)dx \tag{B.16}$$

$$H_{y,i} = -2\int_{-1}^{1} \frac{y_i(x_1)\sqrt{1-{x_1}^2}}{x_1-1} dx_1 \tag{B.17}$$

$$H_{dyd\varepsilon,i} = -2\int_{-1}^{1} \frac{y_i'(x_1)\sqrt{1-{x_1}^2}}{x_1-1} dx_1 \tag{B.18}$$

$$K_{y,i} = -2\int_{-1}^{1} \frac{y_i(x_1)\sqrt{1-{x_1}^2}}{x_1+1} dx_1 \tag{B.19}$$

$$K_{dyd\varepsilon,i} = -2\int_{-1}^{1} \frac{y_i'(x_1)\sqrt{1-{x_1}^2}}{x_1+1} dx_1 \tag{B.20}$$

$$TI1_i = \int_{-1}^{1} \sqrt{1-x_1^2}\, y_i'(x_1)\, dx_1 \tag{B.21}$$

$$TI2_{i,j} = \int_{-1}^{1} f_{y,j}(x_1)\, y_i'(x_1)\, dx_1 \tag{B.22}$$

$$TI3_{i,j} = \int_{-1}^{1} f_{dyd\varepsilon,j}(x_1)\, y_i'(x_1)\, dx_1 \tag{B.23}$$

$$TI4_i = \int_{-1}^{1} x_1\sqrt{1-x_1^2}\, y_i'(x_1)\, dx_1 \tag{B.24}$$

$$TI5_i = \int_{-1}^{1} \frac{x_1-1}{\sqrt{1-x_1^2}}\, y_i'(x_1)\, dx_1 \tag{B.25}$$

$$TI6_i = \int_{-1}^{1} \frac{(2x_1+1)(x_1-1)}{\sqrt{1-x_1^2}}\, y_i'(x_1)\, dx_1 = -2TI1_i - TI5_i \tag{B.26}$$

$$TI7_i = \int_{-1}^{1} \frac{x_1}{\sqrt{1-x_1^2}}\, y_i'(x_1)\, dx_1 \tag{B.27}$$

$$TI8_{i,j} = \int_{-1}^{1} \frac{\partial f_{dyd\varepsilon,j}}{\partial x}(x_1)\, y_i'(x_1)\, dx_1 \tag{B.28}$$

$$TI9_{i,j} = \int_{-1}^{1} \frac{\partial f_{y,j}}{\partial x}(x_1)\, y_i'(x_1)\, dx_1 \tag{B.29}$$

$$PI1_i = \int_{-1}^{1} \sqrt{1-x_1^2}\, y_i(x_1)\, dx_1 \tag{B.30}$$

$$PI2_{i,j} = \int_{-1}^{1} f_{y,j}(x_1)\, y_i(x_1)\, dx_1 \tag{B.31}$$

$$PI3_{i,j} = \int_{-1}^{1} f_{dyd\varepsilon,j}(x_1)\, y_i(x_1)\, dx_1 \tag{B.32}$$

$$PI4_i = \int_{-1}^{1} x_1\sqrt{1-x_1^2}\, y_i(x_1)\, dx_1 \tag{B.33}$$

$$PI5_i = \int_{-1}^{1} \frac{x_1-1}{\sqrt{1-x_1^2}}\, y_i(x_1)\, dx_1 \tag{B.34}$$

$$PI6_i = \int_{-1}^{1} \frac{(2x_1+1)(x_1-1)}{\sqrt{1-x_1^2}}\, y_i(x_1)\, dx_1 = -2PI1_i - PI5_i \tag{B.35}$$

$$PI7_i = \int_{-1}^{1} \frac{x_1}{\sqrt{1-x_1^2}}\, y_i(x_1)\, dx_1 \tag{B.36}$$

$$PI8_{i,j} = \int_{-1}^{1} \frac{\partial f_{dyd\varepsilon,j}}{\partial x}(x_1)\, y_i(x_1)\, dx_1 \tag{B.37}$$

$$PI9_{i,j} = \int_{-1}^{1} \frac{\partial f_{y,j}}{\partial x}(x_1)\, y_i(x_1)\, dx_1 \tag{B.38}$$

Please note that $TI6_i$ can be computed from $TI1_i$ and $TI5_i$, and that $PI6_i$ can be computed from $PI1_i$ and $PI5_i$. The present nomenclature was kept to preserve clarity in the presentation of the results.

The memory term associated with the vorticity shed in the wake can be expressed in an approximative state-space reperesentation

$$Q\mathbf{C} = Q(t)\left(1-\sum_i A_i\right) + \sum_i z_i \tag{B.39}$$

$$\dot{z}_i + b_i\frac{1}{b}(V-\dot{X}(t))z_i = b_i A_i \frac{1}{b}(V-\dot{X}(t))Q(t). \tag{B.40}$$

C Computation of the Deflection Shape Integrals

Since some of the deflection shape integrals requires integration over expressions that are singular, calculation of these require special attention.

$f_{y,i}(x)$ and $f_{dyd\varepsilon,i}(x)$ deflection integrals

The evaluation of the $f_{y,i}(x)$ and $f_{dyd\varepsilon,i}(x)$ deflection integrals require integration with respect to x_1 over the mode shape or mode shape derivative multiplied by

$$\ln\left(\frac{(x-x_1)^2+\left(\sqrt{1-x^2}-\sqrt{1-x_1{}^2}\right)^2}{(x-x_1)^2+\left(\sqrt{1-x^2}+\sqrt{1-x_1{}^2}\right)^2}\right).$$

This expression goes toward $-\infty$ for $x_1 \to x$. However, the integral over this singularity is non-singular. The integrals are can be evaluated using the analytical integrals given in the work by Theodorsen [20]

$$\begin{aligned} II_1(x,x_a,x_b) &= \int_{x_a}^{x_b} \ln\left(\frac{(x-x_1)^2+\left(\sqrt{1-x^2}-\sqrt{1-x_1{}^2}\right)^2}{(x-x_1)^2+\left(\sqrt{1-x^2}+\sqrt{1-x_1{}^2}\right)^2}\right) dx_1 \\ &= 2(x-x_a)\ln N_a - 2\sqrt{1-x^2}\arccos(x_a) \\ &\quad -2(x-x_b)\ln N_b + 2\sqrt{1-x^2}\arccos(x_b) \end{aligned} \tag{C.1}$$

$$\begin{aligned} II_2(x,x_a,x_b) &= \int_{x_a}^{x_b} \ln\left(x_1\frac{(x-x_1)^2+\left(\sqrt{1-x^2}-\sqrt{1-x_1{}^2}\right)^2}{(x-x_1)^2+\left(\sqrt{1-x^2}+\sqrt{1-x_1{}^2}\right)^2}\right) dx_1 \\ &= -\sqrt{1-x_a^2}\sqrt{1-x^2} - x\arccos(x_a)\sqrt{1-x^2} + (x^2-x_a^2)\ln N_a \\ &\quad +\sqrt{1-x_b^2}\sqrt{1-x^2} + x\arccos(x_b)\sqrt{1-x^2} - (x^2-x_b^2)\ln N_b, \end{aligned} \tag{C.2}$$

where N_a and N_b are

$$N_a = \frac{1-x_a x-\sqrt{1-x^2}\sqrt{1-x_a^2}}{|x-x_a|} \tag{C.3}$$

$$N_b = \frac{1-x_b x-\sqrt{1-x^2}\sqrt{1-x_b^2}}{|x-x_b|}. \tag{C.4}$$

If the values of y_i used in the computation of $f_{y,i}(x)$ are approximated by piecewise linear functions, then $f_{y,i}(x)$ can be approximated by

$$f_{y,i}(x) \approx \sum_{j=1}^{N_x-1}\left(A_{i,j}II_1(x,x_j,x_{j+1}) + B_{i,j}II_2(x,x_j,x_{j+1})\right) \tag{C.5}$$

$$A_{i,j} = y_i(x_j) - x_j\frac{y_i(x_{j+1})-y_i(x_j)}{x_{j+1}-x_j}$$

$$B_{i,j} = \frac{y_i(x_{j+1})-y_i(x_j)}{x_{j+1}-x_j}$$

The evaluation of $f_{dyd\varepsilon,i}(x)$ is analogous to the evaluation of $f_{y,i}(x)$. In this case the deflection shape values, $y_i(x)$, are interchanged with deflection slope values, $y_i'(x)$.

$\frac{\partial f_{y,i}(x)}{\partial x}$ and $\frac{\partial f_{dyd\varepsilon,i}(x)}{\partial x}$ deflection integral derivatives

The deflection integral derivative $\frac{\partial f_{y,i}(x)}{\partial x}$ is found by differentiation of Equation (C.5).

$$\frac{\partial f_{y,i}(x)}{\partial x} \approx \sum_{j=1}^{N_x-1}\left(A_{i,j}\frac{\partial II_1(x,x_j,x_{j+1})}{\partial x} + B_{i,j}\frac{\partial II_2(x,x_j,x_{j+1})}{\partial x}\right) \quad \text{(C.6)}$$

The value of $\frac{\partial f_{dyd\varepsilon,i}(x)}{\partial x}$ is computed analogously.

$F_{y,i}(c)$ and $F_{dyd\varepsilon,i}(c)$ deflection integrals

The values of $F_{y,i}(c)$ and $F_{dyd\varepsilon,i}(c)$ can be obtained by a suitable type of numerical integration of the previously computed values of $f_{y,i}(x)$ and $f_{dyd\varepsilon,i}(x)$ from $x = c$ to $x = 1$.

$G_{y,i}(c)$ and $G_{dyd\varepsilon,i}(c)$ deflection integrals

The values of $G_{y,i}(c)$ and $G_{dyd\varepsilon,i}(c)$ can be obtained from $f_{y,i}(x)$ and $f_{dyd\varepsilon,i}(x)$ by a suitable type of numerical integration. One possibility is to assume a piecewise linear variation of $f_{y,i}(x)$ and $f_{dyd\varepsilon,i}(x)$ with respect to x. With this assumption, the result is

$$G_{y,i}(c) \approx \sum_{j=1}^{N_{xc}-1}\left(1/2(x_{j+1}^2 - x_j^2)A_{i,j} + 1/3(x_{j+1}^3 - x_j^3)B_{i,j}\right) \quad \text{(C.7)}$$

$$A_{i,j} = f_{y,i}(x_j) - x_j\frac{f_{y,i}(x_{j+1}) - f_{y,i}(x_j)}{x_{j+1} - x_j}$$

$$B_{i,j} = \frac{f_{y,i}(x_{j+1}) - f_{y,i}(x_j)}{x_{j+1} - x_j}.$$

Again, the evaluation of $G_{dyd\varepsilon,i}(c)$ is analogous to the evaluation of $G_{y,i}(c)$. In this case the deflection shape values, $y_i(x)$, are interchanged with deflection slope values, $\frac{d}{d\varepsilon}y_i(x)$.

$H_{y,i}$ and $H_{dyd\varepsilon,i}$ deflection integrals

As in the cases above, a numerical approximation to the $H_{y,i}$ and $H_{dyd\varepsilon,i}$ integrals can be found employing a piecewise linear approximation of y_i and $dy_i/d\varepsilon$ using the analytical integrals

$$\int \frac{\sqrt{1-x_1^2}}{x_1 - 1}dx_1 = \sqrt{1-x_1^2} - \arcsin(x_1) \quad \text{(C.8)}$$

$$\int x_1\frac{\sqrt{1-x_1^2}}{x_1 - 1}dx_1 = (\frac{1}{2}x_1 + 1)\sqrt{1-x_1^2} - \frac{1}{2}\arcsin(x_1) \quad \text{(C.9)}$$

$K_{y,i}$ and $K_{dyd\varepsilon,i}$ deflection integrals

Numerical approximations to these can be found as above with the help of the following integrals

$$\int \frac{\sqrt{1-x_1^2}}{x_1 + 1}dx_1 = \sqrt{1-x_1^2} + \arcsin(x_1) \quad \text{(C.10)}$$

$$\int x_1\frac{\sqrt{1-x_1^2}}{x_1 + 1}dx_1 = (\frac{1}{2}x_1 + 1)\sqrt{1-x_1^2} - \frac{1}{2}\arcsin(x_1) \quad \text{(C.11)}$$

$TI1_i$, $TI4_i$, $TI5_i$, $TI6_i$ and $TI7_i$ deflection integrals

These deflection integrals may be again computed as the previous, employing the piecewise linear assumption of y_i and $dy_i/d\varepsilon$, with the help of the following analytic integrals

$$\int \sqrt{1-x_1^2}dx_1 = \frac{1}{2}x_1\sqrt{1-x_1^2} + \frac{1}{2}\arcsin(x_1) \tag{C.12}$$

$$\int x_1\sqrt{1-x_1^2}dx_1 = -\frac{1}{3}(1-x_1^2)^{3/2} \tag{C.13}$$

$$\int x_1^2\sqrt{1-x_1^2}dx_1 = -\frac{1}{4}x_1(1-x_1^2)^{3/2} + \frac{1}{8}x_1\sqrt{1-x_1^2} + \frac{1}{8}\arcsin(x_1) \tag{C.14}$$

$$\int \frac{1}{\sqrt{1-x_1^2}}dx_1 = \arcsin(x_1) \tag{C.15}$$

$$\int \frac{x_1}{\sqrt{1-x_1^2}}dx_1 = -\sqrt{1-x_1^2} \tag{C.16}$$

$$\int \frac{x_1^2}{\sqrt{1-x_1^2}}dx_1 = -\frac{1}{2}x_1\sqrt{1-x_1^2} + \frac{1}{2}\arcsin(x_1) \tag{C.17}$$

$TI2_{i,j}$, $TI3_{i,j}$, $TI8_{i,j}$ and $TI9_{i,j}$ deflection integrals

Since the values of $f_{y,i}(x)$, $f_{dyd\varepsilon,i}(x)$ and their derivatives with respect to x can be determined as outlined previously, the integrals $TI2_{i,j}$, $TI3_{i,j}$, $TI8_{i,j}$ and $TI9_{i,j}$can be computed using any suitable numerical integration.

PI deflection integrals

The computation of the PI-integrals, the deflection shape integrals for the computation of the power and modal forces, are analogous to the computation of the TI-integrals. The only difference is that the the slopes of the deflection shapes, y_i', in the TI-integrals are interchanged with the deflection shapes themselves, y_i.

D Velocity Potentials and Analytical Values of the Integrals Used for Computing Deflection Integrals for a Flat Plate With a Flap

The following velocity potentials and integrals can be found in Theodorsen's classic work [20]. Note that the heave coordinate used in the original work, h, which is positive down, is replaced with the heave coordinate used in the present work, Y, which is positive upward.

Velocity Potentials

$$\varphi_\alpha(x) = V\alpha b\sqrt{1-x^2} \tag{D.1}$$

$$\varphi_{\dot{Y}}(x) = -\dot{Y}b\sqrt{1-x^2} \tag{D.2}$$

$$\varphi_{\dot{\alpha}}(x) = \dot{\alpha}b^2(\frac{1}{2}x-a)\sqrt{1-x^2} \tag{D.3}$$

$$\varphi_\beta(x) = \frac{1}{\pi}V\beta b\left(\sqrt{1-x^2}\arccos(c)-(x-c)\ln(N)\right) \tag{D.4}$$

$$\varphi_{\dot{\beta}}(x) = \frac{1}{2\pi}\dot{\beta}b^2\Bigg(\sqrt{1-c^2}\sqrt{1-x^2} + (x-2c)\sqrt{1-x^2}\arccos(c)-(x-c)^2\ln(N)\Bigg) \tag{D.5}$$

where

$$N = \frac{1-cx-\sqrt{1-x^2}\sqrt{1-c^2}}{x-c}$$

Analytical Integrals

$$\int_c^1 \sqrt{1-x^2}dx = \frac{1}{2}\arccos(c)-\frac{1}{2}c\sqrt{1-c^2}$$

$$\int_c^1 \sqrt{1-x^2}(x-c)dx = \frac{1}{6}\sqrt{1-c^2}(2+c^2)-\frac{1}{2}c\arccos(c)$$

$$\int_{-1}^1 \sqrt{1-x^2}(x-c)dx = -\frac{\pi}{2}c$$

$$\int_c^1 (\frac{1}{2}x-a)\sqrt{1-x^2}dx = \frac{1}{6}(1-c^2)^{3/2}+a\left(\frac{1}{4}\arccos(c)-\frac{1}{4}c\sqrt{1-c^2}\right)$$

$$\int_c^1 (\frac{1}{2}x-a)\sqrt{1-x^2}(x-c)dx = \frac{1}{2}(\frac{1}{8}+c^2)\arccos(c)-\frac{1}{16}c\sqrt{1-c^2}(7+2c^2) + \frac{1}{2}(c-a)\left(\frac{1}{3}\sqrt{1-c^2}(2+c^2)-c\arccos(c)\right)$$

$$\int_{-1}^1 (\frac{1}{2}x-a)\sqrt{1-x^2}(x-c)dx = \frac{\pi}{16}+\frac{\pi}{2}ac$$

$$\int_c^1 \sqrt{1-x^2}\arccos(c)-(x-c)\ln(N)dx = \frac{1}{2}(1-c^2)+\frac{1}{2}\arccos^2(c)-c\sqrt{1-c^2}\arccos(c)$$

$$\int_c^1 \left(\sqrt{1-x^2}\arccos(c) - (x-c)\ln(N)\right)(x-c)dx = -\frac{1}{2}c(1-c^2) + \frac{1}{2}\sqrt{1-c^2}(1+c^2)\arccos(c)$$
$$-c\frac{1}{2}\arccos^2(c)$$

$$\int_{-1}^1 \left(\sqrt{1-x^2}\arccos(c) - (x-c)\ln(N)\right)(x-c)dx = \frac{\pi}{6}\sqrt{1-c^2}(2c^2+1) - c\frac{\pi}{2}\arccos(c)$$

$$\int_c^1 \sqrt{1-c^2}\sqrt{1-x^2} + (x-2c)\sqrt{1-x^2}\arccos(c) - (x-c)^2\ln(N)\,dx$$
$$= -c(1-c^2) + \sqrt{1-c^2}(1+c^2)\arccos(c) - c\arccos^2(c)$$

$$\int_c^1 \left(\sqrt{1-c^2}\sqrt{1-x^2} + (x-2c)\sqrt{1-x^2}\arccos(c) - (x-c)^2\ln(N)\right)(x-c)\,dx$$
$$= (\frac{1}{8}+c^2)\arccos^2(c) - \frac{1}{4}c\sqrt{1-c^2}\arccos(c)(7+2c^2) + \frac{1}{8}(1-c^2)(5c^2+4)$$

$$\int_{-1}^1 \left(\sqrt{1-c^2}\sqrt{1-x^2} + (x-2c)\sqrt{1-x^2}\arccos(c) - (x-c)^2\ln(N)\right)(x-c)\,dx =$$
$$-\pi(\frac{1}{8}+c^2)\arccos(c) + \pi\frac{1}{8}c\sqrt{1-c^2}(7+2c^2)$$

Bibliographic Data Sheet **Risø–R–1478(EN)**

Title and author(s)

Unsteady 2D Potential-flow Forces on a Variable Geometry Airfoil Undergoing Arbitrary Motion

Mac Gaunaa

ISBN	ISSN
87–550–3369–5	0106–2840

Dept. or group	Date
Wind Energy Department	July 2006

Groups own reg. number(s)	Project/contract No.

Sponsorship

Partly funded by the Danish Research Council under the ADAPWING project

Pages	Tables	Illustrations	References
52	0	6	23

Abstract (Max. 2000 char.)

In this report analytical expressions for the unsteady 2D force distribution on a variable geometry airfoil undergoing arbitrary motion are derived under the assumption of incompressible, irrotational, inviscid flow. The airfoil is represented by its camberline as in classic thin-airfoil theory, and the deflection of the airfoil is given by superposition of chordwise deflection mode shapes. It is shown from the expressions for the forces, that the influence from the shed vorticity in the wake is described by the same time-lag for all chordwise positions on the airfoil. This time-lag term can be approximated using an indicial function approach, making the practical calculation of the aerodynamic response numerically very efficient by use of Duhamel superposition. Furthermore, the indicial function expressions for the time-lag terms are formulated in their equivalent state-space form, allowing for use of the present theory in problems employing the eigenvalue approach, such as stability analysis.

The analytical expressions for the forces simplify to all previously known steady and unsteady thin-airfoil solutions.

Apart from the obvious applications within active load control/reduction, the current theory can be used for various applications which up to now have been possible only using much more computational costly methods. The propulsive performance of a soft heaving propulsor, and the influence of airfoil camberline elasticity on the flutter limit are two computational examples given in the report that highlight this feature.

Descriptors

Aerodynamics; Airfoils; Deformable Airfoils; Dynamic Stability; Flutter; Unsteady Potential Flow

Available on request from:
Information Service Department, Risø National Laboratory
(Afdelingen for Informationsservice, Forskningscenter Risø)
P.O. Box 49, DK–4000 Roskilde, Denmark
Phone (+45) 46 77 46 77, ext. 4004/4005 · Fax (+45) 46 77 40 13
E-mail: risoe@risoe.dk

Risø's research is aimed at solving concrete problems in the society.

Research targets are set through continuous dialogue with business, the political system and researchers.

The effects of our research are sustainable energy supply and new technology for the health sector.